Influence of ion pseudopotential on the electronic shell structure of metal clusters

J. Lermé, M. Pellarin, B. Baguenard, C. Bordas, J. L. Vialle, and M. Broyer
Laboratoire de Spectrométrie Ionique et Moléculaire, Université Lyon I Bâtiment 205, 43 Boulevard du 11 Novembre 1918, 69622 Villeurbanne Cedex, France
(Received 2 May 1994)

Electronic shell and supershell structures in spherical multiple-shell and liquidlike clusters, taking into account the electron-ion interaction through usual empty-core pseudopotentials, have been investigated for trivalent and alkali species and compared with the conventional jellium model. In the case of multiple-shell structures we find that the jelliumlike electronic shell structure is clearly developed, in spite of the strong inhomogeneities in the ion density. The supershell pattern is, however, strongly dependent on the geometrical structure and pseudopotential parametrization. In the case of a homogeneous ionic distribution, the overall effect of the non-Coulombic behavior of the pseudopotential at short range is reflected through a softness increase of the effective electronic potential, acting as a diffuse jellium. Results about the shell and supershell structures are in better agreement with experiments, as compared to the standard jellium-model predictions. This effective surface softness, arising only from the finite size of the ionic cores, could also partially correct the present disagreement between experiment and jellium calculations with regard to the cluster polarizabilities and surface plasmon frequencies.

I. INTRODUCTION

Since its experimental evidence by Knight *et al.*,[1] the electronic shell structure of valence electrons in simple metal clusters has been the subject of a prolific literature.[2,3] This shell structure is of primary importance in the physics of metal clusters because the size dependence of numerous cluster properties is governed mainly by the change in the density of states of the valence electrons at the Fermi level, as in solid-state physics. The major features of the electronic shell structure emerge naturally from simple cluster models based on mean-field concepts disregarding the discrete structure of the ionic background. Basically, the valence electrons are supposed to move freely in a structureless flat potential well, assumed to have a spherical shape with a radius $R_{N_e}=r_s N_e^{1/3}$, where r_s is the Wigner-Seitz radius per valence electron in the bulk material, and N_e the number of valence electrons. However, the independent-electron ("free motion") hypothesis is not a prerequisite. In the self-consistent spherical jellium background model (JBM),[4,5] the total charge of the ions is uniformly spread out over the volume of a sphere of radius R_{N_e}, and all Coulomb interactions are treated quantum mechanically. Worked out within the density-functional theory (DFT) and the Kohn-Sham (KS) procedure,[6] the resulting equations can be formally considered as dealing with N_e independent electrons trapped in a spherical potential box. In such a potential the individual energy levels $E_{n,l}$ are highly degenerate and tend to group into bunches which are clearly distinct in small clusters. In large clusters, the electron energy spectrum is very congested, but the persistence of a strong state-bunching phenomenon is revealed in the smoothed density of states. As in atomic or nuclear physics, which both deal with fermion systems, the spherical symmetry and the approximate size independence of the level ordering are the two keys for the emergence of the electronic shell structure which arises from the sequential filling of the lowest $2(2l+1)$-fold-degenerate levels (subshells) and the level bunches (major shells) by the N_e valence electrons. Sizes of enhanced stability, called magic sizes, correspond to clusters with closed shells. Quantitatively the level-clustering phenomenon modulating the density of electronic states is reflected through size-dependent shell effects which are periodic on a $N_e^{1/3}$ scale (approximately $\Delta N_e^{1/3}\approx 0.6$ between two consecutive magic numbers). In the large-size domain, theoretical and experimental results show that the shell effects vanish periodically but with a much larger size scale ($\Delta N_e^{1/3}\approx 6$). This effect, called the supershell structure, appears as a beating phenomenon and is interpreted in a very elegant way within the semiclassical theory of the density of states,[7,8] as arising from the interference between the triangular and square closed orbit contributions. In the discrete-level quantum picture the supershell structure results from the progressive shift between two level-bunch series having close periodicities.

All these features have been extensively observed in alkali cluster experiments, and studied by many groups.[2,3,9–11] Globally the experimental results agree almost perfectly with the theoretical predictions of the structureless JBM, particularly in the low size domain.[12,13] Indeed, in small clusters, the gaps between the groups of levels are sufficiently large to prevent some bunch coalescence which could occur when including the granular structure or surface roughness of the clusters, ingredients ignored in usual Jellium-like models. However, some discrepancies have been noticed in the medium and large size ranges and have cast doubts on the standard JBM.[9,14] For example, the experimental beat location in Na_N cluster mass spectra extends around the size $N_e\approx 1000$, above the size domain predicted by standard JBM calculations ($N_e=700-800$). In addition,

discrepancies between various experimental results suggest that the electronic structure depends on the experimental conditions via differences in the cluster geometrical structure[9,15] (see Table I of Ref. 11 for a compilation of the experimental results on alkali species). Nevertheless the discrepancies are rather minor and could easily be erased, without forsaking the basic hypothesis of the JBM (averaging of the ionic charge density), by relaxing the assumed homogeneity of the jellium density,[14] or the arbitrary step-profiled parametrization of the jellium wall.[16] In consequence the JBM remains a suitable model for describing the electronic shell structure of the valence electrons and predicting the magic sizes. However, the above ingredients introduced to correct the discrepancies between theory and experiment are phenomenological (as the step-profiled jellium wall), and are added to the conventional JBM in an *ad hoc* manner, even though some physical effects may be invoked as support.

The same theoretical framework has been successfully applied to more complex elements, where ion pseudopotentials and band-structure effects are stronger, such as noble and group-II *B* elements (filled atomic *d* shell, s^1 and s^2 atomic configurations),[17–20] and trivalent group-III *A* metals (ns^2np^1 atomic configuration).[21–26] The experiments carried out with the trivalent species by Pellarin and co-workers[22–26] have provided additional insight into metal cluster physics. The results seem to indicate that the emergence of a JBM-like electronic structure is closely related to the liquidlike structure of the clusters. In fact these experiments do not strictly prove the liquidlike structure of the clusters over the entire volume. Indeed, one might suspect that the development of the JBM-like electronic shell structure results only from the favored overall shape symmetry: the main consequence of the thermal effects in Ref. 26 being presumably the smoothing or suppression of the unavoidable roughness and faceting of rigid close-packed arrangements (this effect could be related to the surface melting observed in cluster dynamics simulation),[27–29] and the promotion of a perfect spherical shape (this point will be discussed in more detail in Sec. II). In addition, with regard to the electronic shell structure, considerable differences from the alkali species have been observed. The most striking feature is a considerable shift of the beat location, found at much larger cluster sizes ($N_e=2500$ for gallium).[25]

The purpose of this paper is to investigate, through model calculations, how and to what extent the ionic-background discontinuity and the finite ion volume modify the JBM-like electronic shell structure, and could underlie the discrepancies between experiment and JBM calculations. We first attempt to answer the question of whether the usual electronic shell structure, characterized by the shell spacing $\Delta N_e^{1/3}\approx 0.6$, emerges in nonsmooth effective potentials resulting from strongly inhomogeneous ion distributions. For small clusters ($n<25$), in spite of the apparent crudeness of the JBM for describing real clusters, *ab initio* calculations[30–32] preserve the JBM electronic shell structure. Moreover, sophisticated models including both discrete structure and suitable ion pseudopotential,[33–35] also preserve this structure. This is also the case within the Hückel formalism,[36–38] where the lattice geometry is formally taken into account by specifying the nearest neighbors of a given atom, and the elements of the Hückel matrix are derived from accurate molecular calculations.[38] As previously emphasized, the large magnitude of bunch spacings in the zero-order (JBM) approximation explains the weak qualitative influence of the perturbative lattice effects. To our knowledge, no study over a large-size domain has been reported in the literature for large clusters ($N>100$). Obviously the reason is the formidable computational effort required to carry out this challenge when self-consistency of both lattice and electronic structures is prescribed. Confident extrapolation to larger sizes of the agreement between experiments and JBM observed in the small-size range is speculative owing to the congested electronic state density in large clusters. *A priori,* fusion of the level bunches and/or changes in the bunch filling numbers (as compared to the JBM results), induced by the cluster granularity and roughness, are expected. Natural emergence of the size-shell structure in flat electronic effective potential is partially due to the rough scaling law of the energy levels: $E_{n,l}\sim 1/R_{N_e}^2$ (the energy is measured from the bottom of the potential). This approximate radius dependence prevents occurrence of strong reordering of the energy levels when the cluster size varies. In the semiclassical picture the linear relation linking the triangular/square orbit lengths and the cluster radius R_{N_e} is responsible for the shell and supershell structures characterized by a constant spacing between consecutive magic sizes. Intuitively these scaling laws are expected to be very approximate, or even completely wrong, in the case of potentials having a nonflat bottom. Surprisingly, in the case of trivalent metal clusters, the standard JBM-like electronic shell structure (more precisely the shell spacing) is observed by simple eye inspection of unprocessed mass spectra over a very large size domain (up to $N_e=7000$ for gallium),[25] in spite of very strong electron-ion interaction. Therefore, a theoretical study of the actual impact of the discrete ionic structure in large clusters is highly required. With regard to the supershell pattern, it is also advisable to look for the possible granular-structure origin of the discrepancy observed between theory and experiment.

Because the effects of the discrete structure are expected to be more pronounced in nonalkali metals, most of the calculations reported in this paper concern large clusters of trivalent species which are exhaustively studied in our laboratory. A similar study could be undertaken with alkali using the same approach. Our calculations are carried out within the framework of the SAPS (spherically averaged pseudopotential) approximation, which, at the present time, is the only numerically practical technique allowing to deal with very large clusters.[33–35] This approximation, assumed to describe quite well the main effects on the electronic structure arising from the granular background, consists of retaining only the spherical part of the total electron-ion interaction. Support for this numerical approximation will be provided. To avoid the considerable computational time required to determine

the ionic geometry minimizing the cluster energy, approximate but reliable results from the "universal cluster model" developed by Spina and Brack,[39] which is a reasonable extrapolation of the microscopic calculations performed on small clusters within the SAPS approximation, will be used for the ionic structure. A self-consistent calculation of the effective electronic potential will be carried out. Shell energy curves for various ionic configurations and pseudopotential parametrizations will be reported to emphasize the great sensitiveness of the resulting electronic shell structure to model ingredients. Finally, electronic shell structure for homogeneous liquidlike clusters will be investigated.

The paper is organized as follows. In Sec. II we discuss some general questions concerning the emergence of the electronic shell structure in clusters, as well as various simplifying hypothesis usually assumed in theoretical models. In Sec. III we outline the "universal cluster model" of Spina and Brack, with a particular focus on the features relevant to a suitable determination of the electronic shell structure. Results for both multiple-shell and liquidlike clusters are reported in Sec. IV. Concluding remarks and a summary of the major results are given in Sec. V.

II. COMMENTS ABOUT THE EMERGENCE OF THE ELECTRONIC SHELL STRUCTURE IN TRIVALENT METAL CLUSTERS

Recent experiments by Pellarin and co-workers[22–26] have clearly pointed out that the development of the JBM-like electronic shell structure is correlated with the experimental conditions, and undoubtedly with the temperature involved during the cluster growth and photoionization process. They observed that the mass spectra of gallium clusters [melting point T_f (bulk)=303 K] (Ref. 25) exhibit the JBM-related periodicity $\Delta N_e^{1/3}=0.6$, while aluminum clusters [T_f(bulk)=933 K] mass spectra show a periodic pattern ($\Delta N_e^{1/3}=0.31$) which is correlated to the faceting of octahedral fcc clusters.[22,23,40] For indium clusters [T_f(bulk)=430 K] complex mass spectra suggest a strong competition between JBM electronic and geometrical effects. Recently, a more direct relationship with the internal cluster temperature was supported by recording mass spectra of Al_N clusters produced at various source temperatures.[26] By gradually heating the laser vaporization source up to 473 K, Baguenard *et al.* observed a progressive transition from the octahedral to the jelliumlike size periodicity in the mass spectra. In fact, such a change in the cluster structure versus temperature can also be inferred from a comparative examination of previous results obtained with alkali clusters. For instance mass spectra of large cold photoionized Na_N clusters reveal a cuboctahedral or icosahedral geometric cluster structure,[15] characterized by specific magic numbers, from $N=1500$, although subsequent abundance spectra involving warmer clusters exhibit the JBM-like electronic shell structure up to 3000 electrons.[9]

A. On the eventual statistical origin of the electronic shell structure

This correlation, obvious at first glance, raises additional questions related to the emergence of the electronic shell structure in large clusters, and its dependence on the ionic arrangement. Intuitively, it appears that thermal effects favor the spherical symmetry (minimization of the surface energy), prevent the growth of ordered close-packed ionic arrangements, and wipe out—on average—the granular structure of the effective mean-field potential experienced by the valence electrons. However, assuming the above phenomenological picture ("moving disordered ionic lattice") to support theoretical models involving structureless backgrounds rests on an implicit (but nonjustified) hypothesis. Above all, the time scale for an effective ionic density averaging has to be compared with the characteristic time scale of the valence electron motion or of the relevant electronic process involved in a given observable, for instance the time scale of the photoionization process for near-threshold experiments. Indeed the electronic time scales are shorter than those of the ionic degrees of freedom, as is assumed in cluster dynamics simulations (Born-Oppenheimer approximation). That is, the valence electrons encounter essentially a rigid ionic structure, not necessarily perfectly spherical and homogeneous.

Hence the origin of the almost perfect agreement with the conventional spherical JBM (except for the supershell features) could have two distinct explanations: (i) the electronic structure of rigid clusters having nonbulklike or amorphous structures and negligible shape distortion from a perfect sphere does not differ sensibly from the structure obtained within the structureless spherical JBM; (ii) the statistical averaging of the measured electronic shell structure-related observables, arising from the numerous ionic configurations probed when recording an experimental mass spectrum, can be taken into account globally, in a model description, by some shape averaging and a spatial smoothing of the instantaneous effective potential encountered by the electrons.

This paper attempts mainly to test the first hypothesis, although in a schematic way and under the assumption of a perfect spherical symmetry. With regard to the second hypothesis, calculations by Manninen, Mansikka-aho, and Hammaren[41] show that the average density of states from an ensemble of Hückel fcc clusters generated by the Monte Carlo method exhibits the standard closing numbers even if each individual cluster does not. These authors argue that the residual discrepancy with the exact JBM magic numbers could be due to insufficient statistics. However, caution has to be taken when connecting the observable shell structure to some averaged model ingredient, whether time or ensemble averaging, or spatial smoothing. As an illustration, let us consider the simple phenomenological model consisting of a spherical potential well with square wall and finite depth having a radius $R(t)$ oscillating slowly around the value R_{N_e} (total amplitude ΔR). With a typical potential depth the shell structure does not depend on the instantaneous value of $R(t)$, as for the infinite spherical potential box (all the occupied

energy levels $E_{n,l}$ scale approximately according to R^{-2}). Therefore the shell structure will be pronounced and characterized by well-defined magic sizes. By contrast, a time averaging of the instantaneous electron state density displays a rather weakly contrasted shell structure. The modulation in the averaged state density vanishes if $2(dE/dR)\Delta R$ exceeds the level-bunch spacing near the Fermi level. If we assume that the valence electrons encounter only the time-averaged potential (hypothesis of a long electronic time scale) the resulting effective potential has now a soft surface wall (thickness ΔR). Such a potential profile leads to noticeable shifts (depending on the ΔR value) of the node and antinode locations in the supershell structure, as compared to the steep wall case. Identical results are obtained if the averaging of the state density or the effective potential is performed from an ensemble of rigid clusters having a finite radius-distribution width. This academic example stresses that finding a simple theoretical proof for the statistical-averaging origin of the successful development of the JBM shell structure is not a trivial challenge. From the above example we see that improper averaging procedure could lead to wrong predictions, which in addition depend on the physical quantity selected to perform the model averaging.

B. On the spherical symmetry

In all cases, theoretical calculations indicate that the observation of the JBM-like electronic structure is inconsistent with models involving rigid closed-packed clusters[37] (even those built to ensure the most perfectly a spherical shape) or phenomenological models involving a polyhedral faceted potential boundary,[42] except for small clusters (roughly $N<300$ for fcc Hückel clusters and $N<500$ for the icosahedral symmetry of the potential box). In both cases, one cause of the discrepancies is the pronounced surface roughness or departure from the spherical shape, which prevents the development of the standard JBM level bunching in the neighborhood of the Fermi level when large clusters are involved. In the case of the simple topological Hückel model, the large departure arises undoubtedly from the intrinsic different nature of this approach as compared to JBM-like models. In particular, in such a formalism, the JBM-like state density is never observed near the Fermi level for $N>300$, and thus simple Hückel models cannot lead to the observed size-shell structure.

Hence JBM-like shell and supershell structures, experimentally observed up to 7000 valence electrons for gallium, seem consistent only with models involving a quasiperfect spherical effective potential. However, we know from the Jahn-Teller theorem that for nonmagic sizes the total cluster energy is lowered by allowing distortion (for instance ellipsoidal) of the spherical overall shape. Self-consistent calculations on small clusters, and experience from nuclear physics, corroborate this feature.[43–45] The relative distortion is expected to decrease versus the cluster size, owing to the decreasing relative magnitude of the shell-correction energy as compared to the liquid-drop-model surface and curvature energies. Moreover, neglecting the granular structure and surface corrugation[42] (two assumptions for usual JBM-like models which ensure the highest state degeneracy and consequently the largest gaps) leads to an overestimate of the shell effects. We have carried out model calculations involving weak-amplitude sinelike surface corrugation of hard-walled spherical potential wells. The results clearly show that the standard electronic shell structure is preserved but weakened, with negligible changes in the magic sizes (see Sec. III A). Similarly, calculations by Genzken and Brack,[46] taking into account electronic excitations induced by finite temperature, lead to a strong smearing out of the shell effects. Nevertheless, all the calculations involving relaxation of the spherical constraint and ellipsoidal deformations show that the change consists mainly of a reduction of the amplitude of the shell effects with no change of the major shell closing numbers. Therefore, as far as prediction of the main magic sizes is concerned, the spherical symmetry, assumed for all sizes, can be considered as a suitable pragmatic assumption.

C. On the beat shift of the supershell structure

The second striking finding arising from the trivalent metal experiments is the considerable discrepancies between experimental and theoretical (JBM) supershell beat locations for these species. The first beat location is found near $N_e=2500$ and 1150, respectively, for gallium clusters.[25] Our recent experiments on warmed aluminum clusters show a similar departure from the JBM predictions: no beat or half-period shift of the magic sizes is observed below $N_e=2000$.[26] In addition, no clear or easily reproducible shell or supershell pattern is obtained in the large-size domain, suggesting a much greater dependence of the Al_N electronic shell structure (and implicitly geometrical structure) on the experimental conditions, as compared to gallium clusters. For both species, the magic numbers in the small-size region are close (although slightly shifted) to the theoretical ones.

In a previous paper we suggested that a slight increase of the surface softness of the effective potential probed by the valence electrons could explain the observed experimental results.[16] Introduction of a suitable jellium softness and complete self-consistent calculations leads to results identical to those of the phenomenological study reported in Ref. 16. Indeed, introduction of a diffuse jellium is not a new ingredient and was previously used by several authors in the scope of the optical response of metal clusters.[47–50] In the field of condensed matter, some works indicate that liquid metal-vapor interfaces are characterized by a smooth positive charge distribution,[51,52] with a thickness on the order of one or two atomic layers. Moreover, generalization by Allen and Rice of the jellium-metal surface model developed by Lang and Kohn,[53] involving mutually self-consistent ionic and electronic charge distributions, leads to smooth jellium walls.[54] However, let us point out that Refs. 51 and 52 are devoted to thermodynamic properties of liquid-metal surfaces and consequently the distributions are derived from ensemble-averaged (or time-averaged according to the ergodic hypothesis) ionic charge distributions.

Therefore, according to the discussion in Sec. II A, these results have to be taken with great care as quantitative support for defining the smooth effective surface potential leading to the observed shell structure. With regard to the relaxed jellium model of Ref. 54, it is obvious that, in spite of the energetic term introduced to stabilize the jellium at a specific metal density in the inner region of the metal slab, the long decreasing tail of the surface jellium distribution is a consequence of the bulk jellium instability (the volume energy in the single-parameter JBM is minimum around $r_s=4.3$ a.u.). For instance, the width of the surface profile for $r_s=4$ a.u. (sodium) is on the order of 11 a.u. With such a diffuse boundary, the first beat location of the supershell structure would be shifted at gigantic cluster size, and moreover the triangular orbit-related shell structure would be destroyed in the small- and medium-size domains. Contrary to these unsuitable results, an increase of the softness of the effective potential at the cluster surface could be explained by a slight static expansion of the outer spherical ionic shell or by large vibrational motion of the surface atoms toward the vacuum (a feature observed in cluster dynamics simulations). On the other hand, the effect of short-wavelength surface roughness, thought to be suitably modelized by a soft ion profile (spatial averaging assumption), would require support from microscopic quantum calculations, as for the inner granularity. Support for this numerical approximation is given in Sec. III A, and the apparent contradiction with our calculations involving corrugated potential box is discussed in Sec. IV D (we stated previously that the main effect of corrugation is a weakening of the shell effects; see Sec. II A).

In this paper we will investigate the influence of rigid discrete ionic distributions, assumed to be spherical, on the electronic shell and supershell structures, with particular emphasis on the beat locations. In order to obtain results intrinsic to the strongly inhomogeneous multiple-shell structure, or to the finite core volume in liquidlike clusters, neither explicit soft distribution nor implicit effective surface softness introduced via some increase of the spacing between the outermost ionic layers are included in our simple models.

III. THE MODEL

A. Ionic structure in the spherically averaged pseudopotential (SAPS) approximation

Our model is derived from results obtained in the SAPS approximation. This simplifying method was introduced by Iniguez *et al.*[33,34] and Mañanes *et al.*[35] in order to include the effects of the discrete ionic structure through appropriate ion-core pseudopotentials. We recall that the purpose of the pseudopotential concept, based on the rigid-core assumption, is to avoid the explicit introduction of the ionic core and of the inner-shell electrons in the electronic quantum calculations. The SAPS technique, still simple enough to be applied to medium-size clusters (roughly up to a few hundred atoms), can be considered as a first-order correction to the drastic structureless spherical JBM and seems to bring a reliable improvement to the JBM. In the SAPS approximation the Coulomb interaction between point-like ions is treated exactly, while the electron cloud is supposed to encounter only the spherical average of the total ion pseudopotential $[V^{ps}(r)]$, which is assumed to be local in this paper as in previous works. This last approximation is equivalent to stipulating the constraint of using only a spherically symmetric electron density in the DFT. This hypothesis is likely to be better justified for large spherical clusters, involving no pronounced large-scale angular-dependent background inhomogeneity. For instance, the SAPS method is expected to be wrong in the case of slight ellipsoidal deformation, or polyhedral potential box models.

This approximation, assumed in Refs. 33–35, can roughly be supported by a simple perturbative approach. The total pseudopotential is expressed according to $V^{ps}=V^{ps}(r)+V'^{ps}(r,\theta,\varphi)$, where the second term, the multiple expansion of the total pseudopotential, is responsible for the breakdown of the spherical symmetry. At the lowest order of the perturbation theory, and with no attempt at self-consistency, the effect of $V'^{ps}(r,\theta,\varphi)$ on the $2(2l+1)$-fold degenerate subspace corresponding to the KS level $E_{n,l}$ consists of a level splitting with no shift of the average energy since the total electron density associated with this level is only r dependent, and the spherical average of $V^{ps}(r,\theta,\varphi)$ is, by definition, equal to zero. The same conclusion holds true if we consider the larger subspace associated with a level bunch, instead of a single KS level. In consequence, the nonspherical part of V^{ps} is expected to produce essentially a weakening of the shell effects through an effective level broadening, with no noticeable change of the shell and supershell closing numbers. Our model calculations involving sinelike corrugation, performed beyond the above perturbative approach, corroborate this statement. We want to stress that the above analysis proves that the SAPS technique is suitable for estimating the electronic shell structure for a given cluster geometry, but not necessarily for optimizing the ionic arrangement.

Microscopic (i.e., the location of each ion is relaxed individually) calculations of the $T=0$ K equilibrium configurations, carried out by minimization of the total cluster energy using the KS-DFT procedure, show that the ions arrange in approximate spherical layers around the cluster center. The geometrical shells are clearly separated along the radial coordinate, with typical radial widths of about 20% of the mean intershell spacing. Such an overall structure exhibits an evident analogy with the multiple-shell structure of rigid closed-packed polyhedral clusters.[55] Obviously the spherical constraint on the electron density favors nested ionic configurations with the same symmetry. However, it is obvious that, by imposing an overall spherical shape to the cluster (an assumption required for ensuring the development of the JBM-like shell structure), the surface atoms are necessarily organized into an outer spherical layer which induces to some extent the same trend inside the volume region. Eventually the emergence of a bulklike core for very large clusters might destroy a deep development of the

spherical arrangement in the inner region.

We believe that finite-temperature microscopic calculations in the SAPS approximation would lead to such a spherical structure for moderate temperatures. In fact, surface ordering is not inconsistent with the liquid state, and some works dealing with liquid metal-vapor interfaces in planar geometry support this kind of structure.[56] It is found that the ion density as a function of the coordinate perpendicular to the interface exhibits strong oscillations extending over several atomic layers into the bulk liquid. The amplitude of these oscillations decreases with increasing temperature and distance from the surface. As previously pointed out, such profiles are indeed averaged thermodynamic distributions. Nevertheless, from the simple requirement of self-consistency with the planar symmetry constraint prescribed for the interface, we believe that these oscillations reflect the actual layer structure of most of the instantaneous configurations of the surface atoms. Another inducing mechanism suggested in order to explain the ordering at the interface is the existence of Friedel oscillations in the electron density close to the surface. Similar ordering, characterized by a strong and damped oscillating atomic distribution, is also obtained in model calculations involving a hard-sphere fluid in contact with a soft repulsive wall.[57]

B. Extrapolation to large clusters

In spite of their relative simplicity, microscopic SAPS calculations are presently limited to rather small clusters with regard to the supershell pattern. To allow application of the above concepts to larger clusters, Spina and Brack[39] developed a simple structural model which incorporates, as prior assumptions, the main qualitative result obtained by Iniguez *et al.*, i.e., the overall multiple-shell structure. Their phenomenological model yields results in good agreement with the microscopic SAPS calculations carried out on small- and medium-size clusters. We outline the basic features of this model which are relevant for our own investigations. In particular, we emphasize eventual changes to be expected between monovalent and nonmonovalent species. We consider below a monovalent metal cluster containing N ions and $N_e=N$ valence electrons. Spina and Brack assume that the ions are homogeneously distributed on perfect spherical shells. We note N_j and R_j the population and the radius of the jth geometric shell (with $R_{N_e}>R_1>R_2>\cdots>R_p$). For simplicity the electron density $n_e(r)$ is assumed to be uniformly distributed over a sphere of radius R_{N_e}: $n_e(r<R_{N_e})=n_0$, where n_0 is the bulk mean value. The ionic structure $\{R_j,N_j\}$ is obtained by minimization of the Madelung energy which includes the major part of the structural dependence:

$$E_{\rm mad}=\sum_{i<j}\frac{N_iN_j}{R_i}+\sum_j E_j(N_j,R_j)+\int n_e(r)\left[\sum_j V_j^{\rm ps}(r)\right]d\mathbf{r}\ . \tag{1}$$

The first term represents the interaction energy among the different shells. This expression, derived by assuming uniform surface charge distributions over the spheres, is a good approximation for evenly distributed pointlike ions, especially for large clusters. The self-energy E_j of the jth sphere is expressed as $N_j(N_j-1)/2R_jf(N_j)$ with a parametrized effective mean interionic distance $Rf(N)$ fitted on energetically favorable discrete configurations. The last term represents the total electron-ion interaction, where $V_j^{\rm ps}(r)$ is the spherically averaged pseudopotential of the jth spherical layer. As in Refs. 33–35 and 39, we use an empty-core parametrization of the ion pseudopotential, extensively used in condensed-matter physics since its introduction by Ashcroft.[58–60] This pseudopotential is purely Coulombic beyond the empty-core radius r_c and takes the constant value A inside the core. In Refs. 33–35 and 39 the radius r_c is matched in order to give a reasonable ionization potential of the corresponding neutral atom. For nonmonovalent species the sum of the successive ionization potentials of the complete atomic valence shell has to be approximately fitted. The spherical average, around the center of the cluster, of the total pseudopotential arising from the N_j ions evenly spaced on the jth sphere is expressed as $V_j^{\rm ps}(r)=N_jv^{\rm ps}(r,R_j)$, with

$$v^{\rm ps}(r,R_j)=\begin{cases}-\dfrac{Z_v}{R_j}, & 0<r<R_j-r_c\\[2mm] -Z_v\dfrac{(r+R_j-r_c)}{2rR_j}+A\dfrac{(r_c^2-(R_j-r)^2)}{4rR_j}, & |R_j-r_c|<r<R_j+r_c\\[2mm] -\dfrac{Z_v}{r}, & r>R_j+r_c\\[2mm] A, & 0<r<r_c-R_j\ .\end{cases} \tag{2}$$

A is the constant value assumed over the ionic core ($A=0$ in the usual Ashcroft parametrization), and Z_v is the valence.

We make the following two remarks: (i) the step-profiled electron distribution provides a scaling factor for the radial coordinate through the R_{N_e} value; and (ii) for actual elements the ion-core volume is much smaller than the mean atomic volume ($r_c/r_a<2$, where r_a is the

Wigner-Seitz radius *per atom* in the bulk). From these, the minimization of Eq. (1) leads to a set of structural parameters $\{N_j, R_j/R_{N_e}\}$ which depend weakly on the element-dependent parameters r_a and r_c. To a very good approximation the spacing d between consecutive shells and the positive charge per surface unit of the spherical layer $\sigma = Z_v N_j / 4\pi R_j^2$ do not depend on the shell indexes and the cluster size N, but obviously depend on the element through the r_a value. These features agree perfectly with recent microscopic SAPS calculations performed by Blundell and Guet on the three-concentric-shell Li_{139}^+ cluster.[61] Such results ensure a constant average radial charge density. Quantitatively the calculations of Spina and Brack lead to the approximate formula $\sigma r_a^2 = 0.35$ (0.03) for a monovalent species, from which the intershell spacing d can be deduced approximately from the planar surface limit equation $d = \sigma / n_0$. The optima shell populations N_j are not necessarily integer numbers in this continuous model. An integer-number constraint could easily be added. Let us emphasize that the resulting errors are not very serious and do not modify the main features reported in Sec. IV, especially since the clusters involved are very large.

Let us now consider a nonmonovalent element of valence Z_v having the same r_a and r_c parameters. Disregarding the A-dependent term in Eq. (2) (a term of the order of $1/R_j^2$, except for the minor contribution of ions located at the center), from direct inspection of Eqs. (1) and (2) it is clear that each term in the Madelung energy Eq. (1) has only to be multiplied by Z_v^2. We conclude therefore that the structural parameters N_j and R_j/R_{N_e} minimizing E_{mad} (for a given N value) are the same as those calculated with $Z_v = 1$. The positive charge density per surface unit σ and the Wigner-Seitz radius per valence electron $r_s = r_a Z_v^{-1/3}$ are then linked by the general equation $\sigma r_s^2 = 0.35 Z_v^{1/3}$.

As a numerical example the intersphere spacing d calculated from the planar surface limit equation is 5.76 and 4.38 a.u. for sodium and aluminum clusters, respectively. It would be advisable to check that these values are, to some extent, consistent with the corresponding parameters of the species in the bulk. Calculations show that the most densely packed cleavage planes lead to the smallest surface energy. Interplanar spacing between consecutive (110) planes for sodium (bcc bulk structure) and (111) planes for aluminum (fcc bulk structure) are 5.64 and 4.41 a.u., respectively. These values are close to the corresponding intersphere spacings. Since in both cases the average charge density is bulklike, the surface charge densities of the cleavage planes and spheres are also similar.

The multiple-shell structure involved in our calculations is then built by nesting concentric ionic shells of radius R_j and positive charge $Z_v N_j = \alpha R_j^2$, with a constant spacing d. The constant α is fixed by the total positive charge constraint. The outermost shell (shell of index 1) is assumed to be located at $R_1 = R_{N_e} - d/2$. This prescription is only approximately ensured in the results reported by Spina and Brack, and is assumed in the Lang and Kohn theory of simple metal surfaces where lattice effects are included via perturbative techniques.[53] By allowing relaxation of the outer lattice plane, these authors found that the relative change of the spacing between the two outermost planes is very small (less than 1% for aluminum), suggesting the reliability of the prescribed location. Actually the absolute value of R_1 is of no importance for our investigations, because in Sec. IV the electronic effective potential will be calculated in a self-consistent way: the choice of the R_1 value with respect to the radius of reference R_{N_e} only sets the overall radius of the effective potential and thus has no effect on the surface pattern of the potential. A tiny change of the global cluster radius has no influence on the electronic shell structure (as a slight change of the r_s value in the JBM). This also holds true with respect to the exact shell spacing d. With regard to the innermost ionic shell of radius R_p, our simple model leads to unphysical situations for particular cluster size ranges (for instance, when $R_p < r_c$), and it would be more satisfactory to change slightly the radius of this shell (set $R_p = 0$), or (if $N_p > 1$) redistribute $N_p - 1$ ions on the other shells. For large clusters, such model refinements, such as the constraint of integer values of the N_j's have a negligible impact on the electronic shell structure. Actually, the ionic structure close to the center of the cluster has little effect on the electronic shell and supershell structures, which are governed mainly by levels of high angular momentum. This statement is easily deduced within the semiclassical picture: the major closed orbits involved in the shell structure lie far from the cluster center (roughly $r > R_{N_e}/2$).

C. Spherically averaged ion pseudopotential

In order to provide insight into the specific features arising from the multiple-shell structure of the clusters, we have calculated the spherically averaged total pseudopotential $V^{\text{ps}}(r)$ for various cluster sizes. Figure 1 displays typical results obtained for sodium and aluminum (all the parameters used throughout this paper are listed in Table I). Since for large clusters the discrepancy with the potential $V^{\text{jel}}(r)$ produced by a uniformly charged hard-walled jellium of radius R_{N_e} is almost imperceptible, only the difference $V^{\text{ps}}(r) - V^{\text{jel}}(r)$ is plotted in Fig. 1 (the differences are on the order of 1% of the absolute value for the displayed sizes). As in planar metal surface studies using empty-core parametrization of the electron-ion interaction, the difference between the total ionic pseudopotential and that from a uniform positively charged background is a periodic function (spatial period d) characterized by two series of bumps which correspond to the successive ionic shell and intershell regions.[53] Specific features are observed in the present case: the periodic oscillation, which exhibits a weakly r-dependent amplitude, is superimposed on a mean curve having a finite positive slope, and very large cusps or dips near the center of the cluster (depending on the cluster size through the R_p value) are observed. These differences are consequences of the spherical geometry

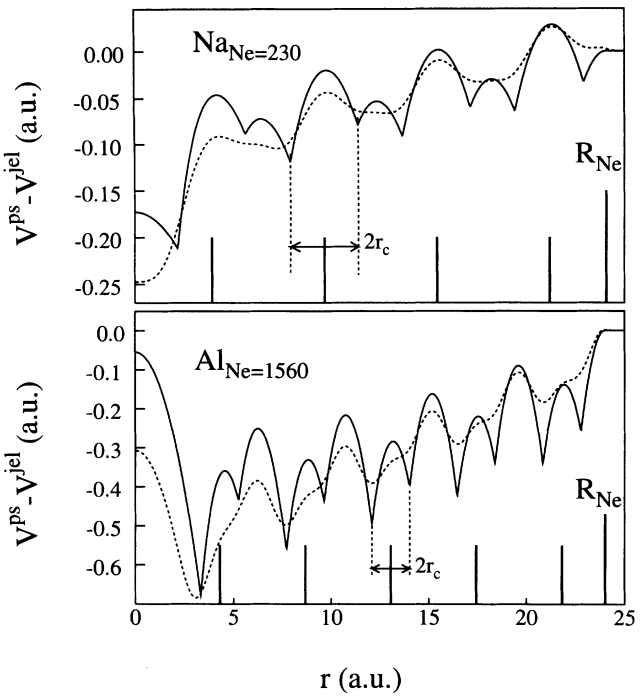

FIG. 1. Difference between the spherically averaged total pseudopotential of multiple-shell clusters and the conventional jellium model ion potential. Empty-core parametrization of the electron-ion interaction is assumed: $r_c=1.74$ and 0.97 a.u. for sodium and aluminum, respectively. The locations of the evenly spaced ionic shells are indicated by vertical lines at the bottom of each figure. Solid curves correspond to ionic structures involving zero-width spherical layers. Dashed curves correspond to ionic structures involving broad layers (a truncated Gaussian radial ion distribution having a FWHM equal to $0.3d$, where d is the layer spacing).

and the finite cluster size. Let us note that very slight changes of the shell populations modify appreciably these specific features. For instance, moving one ion from one shell (index j) to another one (index k) produces the pseudopotential change $Z_v(1/R_j-1/R_k)$ inside the region $r<\min(R_j,R_k)-r_c$. The profile of the mean curve is then noticeably dependent on the ionic populations in each spherical layer. Nevertheless, as will be shown in Sec. IV, large scale fluctuations of $V^{ps}(r)-V^{jel}(r)$ are efficiently screened by very slight inhomogeneities in the average electron density, and the self-consistent electronic effective potential will have a practically constant average value inside the cluster, as in the conventional JBM. Hence we can reasonably assume that the mean curve profile has a minor influence on the electronic shell structure, as compared with the strong and regular size-independent oscillations, which, in contrast with the mean curve, are almost insensitive to minor changes in the structural parameters R_j and N_j. Support for this assertion can be found in Ref. 62, where the electronic shell structure obtained by assuming a perfectly constant potential bottom is found to be identical to the one obtained from complete self-consistent JBM calculations, although the JBM effective potential exhibits slow size-dependent modulations around the average value in the region $r<R_{N_e}$. With regard to the strong cusps or dips at $r\approx 0$, which are spurious features of the SAPS technique near the cluster center, let us stress that only a small cluster region is concerned. Actually this radial domain affects only the very low-angular momentum KS levels, and hence does not perturb the overall shell and supershell structures.

In order to take into account the finite-width ion distribution in each spherical layer observed in $T=0$ K SAPS calculations, and also to simulate some broadening induced by temperature, we have performed calculations with N_j-normalized continuous functions $f(R-R_j)$ describing this broadening. The contribution of the jth ionic layer to the total pseudopotential is then expressed as

$$V_j^{ps}(r)=\int f(R-R_j)v^{ps}(r,R)dR \ . \tag{3}$$

The dashed curves in Fig. 1 illustrate results for such ionic structures (truncated Gaussian profile). As expected, broadening the radial distribution of the ions leads to (i) a smoothing of the pseudopotential cusps or oscillations, and (ii) a progressive vanishing of the Fourier components of the pattern having radial periods shorter than d. We note that the ionic shells and the major positive bumps in the oscillating pseudopotential curve are in phase in the case of sodium, and π shifted in the case of aluminum. This is particularly evident in the case of widened ionic layers. These features are consistent with the microscopic SAPS calculations, where it is observed that the maxima in the radial electron density are located between the ionic shells in alkali systems, and on the ionic shells in trivalent systems.[35,63]

TABLE I. Numerical parameters used in the calculations. r_s is the Wigner-Seitz radius per valence electron, deduced from the bulk density. r_c is the ionic radius. (a) Empty-core radius obtained by Ashcroft to reproduce bulk properties of simple metals (Refs. 58 and 59). (b) Empty-core radius obtained by fitting the atomic ionization potentials (Refs. 33 and 61). (c) Ionic radius ensuring the bulk stability at the actual r_s value, namely $dE/dr_s=0$, where $E(r_s,r_c)$ is the bulk energy functional. We have used the expression reported by Ashcroft and Langreth (Ref. 59), with the electrostatic term corresponding to the liquid structure, and a band-structure term assumed equal to zero. (d) Crystal ionic radius (Ref. 75).

		r_c (a.u.)			
Element	r_s (a.u.)	a	b	c	d
Na	3.93	1.67	1.74	1.68	1.83
Li	3.248	1.06	1.75	1.28	1.28
Al	2.07	1.12	0.97	1.08	0.96
Ga	2.191		0.97	1.17	1.17

IV. RESULTS

A. Evidence for JBM-like electronic shell structure

Assuming multiple-shell structure of the clusters, the Kohn-Sham equations for the density-functional theory are solved self-consistently using Wigner's interpolation

formula for the exchange-correlation energy and the electron-ion interaction Eq. (2). Typical results for both narrow and widened ionic spherical distributions are displayed in Figs. 2 and 3, respectively. Radial electron density (upper figures) and electronic effective potential (lower figures) are compared with JBM results (dashed dotted curves).

As was predicted, the electronic cloud is preferentially concentrated over the attractive spherical ionic layers, and the electronic surface distribution is slightly steeper than the JBM one, a feature already noted by Rubio, Balbas, and Alonso.[63] With regard to the effective potential, we note that cusps in the total ion pseudopotential, characterized by Fourier periods shorter than or comparable to the Fermi wavelength, are reflected with no discernible change, contrary to the long-scale increasing trend which is almost completely erased (see Fig. 1).

Qualitative information about the shell and supershell structures can be obtained by looking at the KS density of states (DOS) of a sufficiently large cluster. In particular, the location of the beat pattern in the DOS, relative to the Fermi level, gives rough information about the size-beat location relative to the cluster size selected. This relationship can be deduced in a straightforward way within an independent-electron model involving a potential having a flat potential bottom and a steep potential wall. In such a potential box the energy levels $E_{n,l}$ pack down approximately as $1/R_{N_e}^2$ with increasing sizes, and the Fermi energy oscillates around the mean bulk value. Because no dramatic reordering of the levels occurs versus the cluster size, the modulations in the cluster observables as a function of the cluster size are directly correlated to the DOS shell structure in the neighborhood of the Fermi level.

KS-DOS, corresponding to the effective potentials of Figs. 2 and 3, are plotted in Figs. 4(b) and 4(c), respectively, and compared to the JBM results [Fig. 4(a)]. The

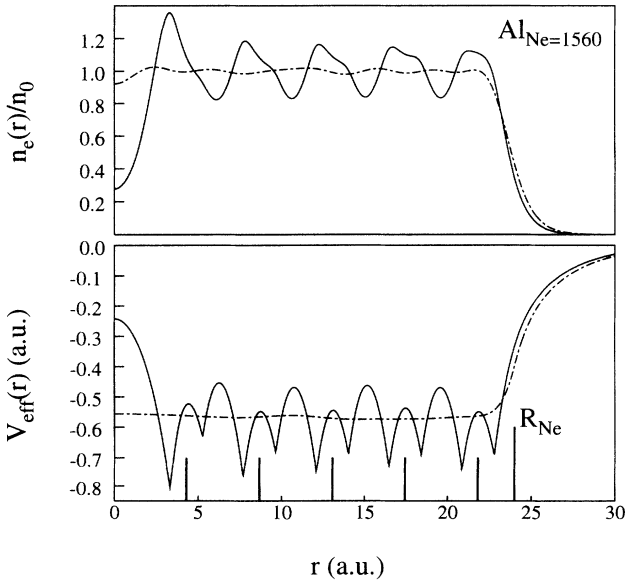

FIG. 2. Self-consistent electronic density (upper figure) and Kohn-Sham effective potential (lower figure) for aluminum clusters having a multiple-shell structure. The total ion pseudopotential is plotted in Fig. 1 (full curve). The location of the zero-width spherical ionic layers are indicated by vertical lines in the lower figure. The dashed-dotted curves correspond to the results of the conventional jellium model.

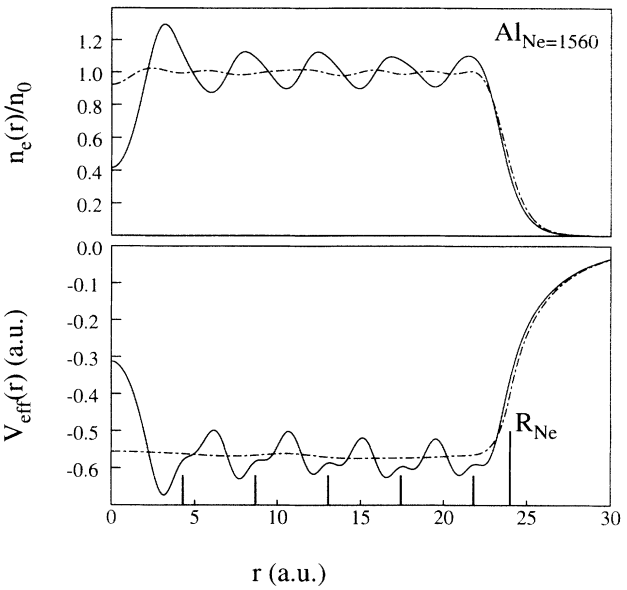

FIG. 3. Same as Fig. 2, but for broad ionic layers (a truncated Gaussian radial ion distribution having a FWHM equal to $0.3d$, where d is the layer spacing).

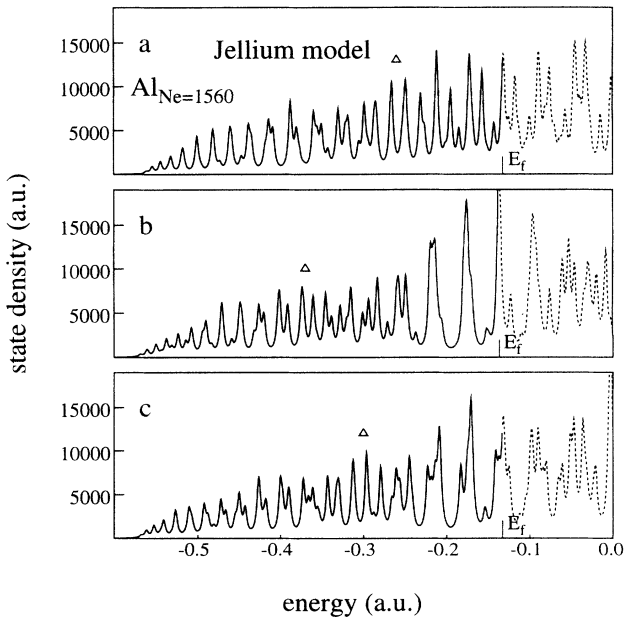

FIG 4. The density of Kohn-Sham states (DOS) for the aluminum cluster Al_{520} ($N_e = 1560$). The electronic effective potentials are displayed in Figs. 2 and 3. (a) DOS obtained with the conventional jellium model. (b) DOS obtained with zero-width concentric ionic layers. (c) DOS obtained with broad ionic layers (a truncated Gaussian radial ion-distribution having a FWHM equal to $0.3d$, where d is the layer spacing). Approximate locations of the beat pattern are indicated by triangles.

discrete DOS have been smoothed in order to more clearly exhibit the main structures of the level grouping. This figure clearly shows that, in spite of the high cusps or periodic distortions modulating the bottom of the effective potential, a strong level-bunching phenomenon, characterized by the same bunch spacing as the one observed in the JBM, occurs. Let us recall that the bunch spacing is constant only on an $E_{\rm kin}^{1/2}$ scale in flat potential models. However the subshell structure is very different compared with the JBM, and depends on the ionic distribution. Approximate locations of the supershell beat in the DOS, characterized by frequency doubling of the peak pattern, are marked with triangles in Fig. 4. The large differences between the various beat locations indicate that the supershell structure is highly dependent on the geometrical cluster structure. Comparison with the JBM results suggests that the size-beat location occurs at lower sizes in the case of well-contrasted spherical multiple-shell structure. Quantitative estimation of the size-beat shift from a particular size-selected DOS requires evaluation of the number of states lying between the beat and the Fermi level. Contrary to models involving a hard-walled constant potential well, we know that this procedure leads to wrong results in general because of the breakdown of the scaling law $E_{n,l}=1/R_{N_e}^2$. For instance, in the case of soft potential profiles, the DOS shell structure depends on the cluster size through the size dependence of the birth of the various classical closed orbits.[16,62] Such a failure is expected in the present case which involves strongly distorted potentials, where the existence and distortion of perfect polygonal orbits are functions of the cluster size through the number of crossed ionic layers during the closed classical path.

B. Shell-correction energy curves

In order to investigate the electronic shell and supershell structures over extended cluster size domains, and for numerous ionic layer distributions, we have applied the efficient independent-electron method (much less time consuming than the JBM), which was successfully tested in Refs. 62 and 64. In the paper by Clemenger, JBM potential profiles calculated for flat metal surfaces by Lang and Kohn[53] were used to study the r_s dependence of the electronic shell structure. This "phenomenological" approach, which in fact includes the size-independent features provided by self-consistent results, was found to generate the same shell structure and magic sizes as those given by self-consistent JBM calculations over the entire size domain. First we calculated self-consistent electronic KS potentials for several large clusters and checked that the potential surface profile was almost size independent, as in the conventional JBM. This general result is due to the fact that the surface profile depends mainly on the quasi-level-independent shape of the decreasing tails of the filled KS wave functions inside the classically forbidden region, and therefore is not noticeably influenced by the electronic shell structure, contrary to the potential shape in the interior. The quasiperiodic cusp pattern modulating the potential bottom is also almost size independent. Actually the tiny differences observed are consequences of the electronic shell structure and can be disregarded, as was proved in Ref. 62. Therefore, the radial effective potential for a given size N_e is expressed according to the functional form $V_{N_e}(r)=\mathcal{V}(r-R_{N_e})$, where $\mathcal{V}$ is built from the self-consistent potential of some large cluster (size N_{e0}). More precisely the effective potential is constructed by the following procedure.

(i) $V_{N_e}(r)=V_{N_{e0}}(r-R_{N_e}+R_{N_{e0}})$ for $r>R_{N_e}-2d$.

(ii) The quasiperiodic cusp pattern is extended below $R_{N_e}-2d$ by repetition of the $V_{N_e}(r)$ profile previously defined in the radial region $[R_{N_e}-2d, R_{N_e}-d]$.

This phenomenological potential does not reproduce the large central bumps or dips (see Figs. 2 and 3). However, inappropriate continuation of our convenient parametrization up to $r=0$ does not distort the results. This will be proved below. Phenomenological potentials for both narrow and widened ionic distributions are plotted in Figs. 5(b) and 5(e) respectively.

Electronic shell structures in such potentials are then derived by calculating the so-called shell-correction energy. This theoretical observable, which exhibits the major magic sizes as pronounced dips, is obtained by subtracting from the cluster energy the average part parametrized as a liquid-drop-model expansion (third-order polynomial in $N_e^{1/3}$). We recall that in independent-electron models, the energy is taken as the sum of the energies of the N_e lowest states. Shell-energy curves, corresponding to the effective potentials drawn in Figs. 5(b) and 5(e), are displayed in Fig. 6, curves *b* and *e*, and compared with the phenomenological JBM-like results [Figs. 5(a) and 6, curve *a*]. The inspection of these curves corroborates the rough indications provided by the DOS curves displayed in Fig. 4 about the supershell structure. The same size shell periodicity as the one obtained in the standard JBM develops in spherical multiple-layer ionic structures. In particular the major magic numbers N_e^* are practically identical in the small-size domain: $N_e^*=9$, 18–21, 39, 57–60, 93, 138, 198, 255–273, 339, and 441. Quite good agreement is also observed in the large-size domain, obviously in size regions corresponding to an even difference between the index numbers of the antinode regions of the supershell pattern. This alternative π and 2π shift of the oscillating shell energy curves is readily visible in Figs. 6(a) and 6(b). The location of the beating pattern, indicated by triangles, differs from the JBM prediction (approximately $N_e=1150$) and depends on the ion distribution (roughly $N_e=500$ and 750 for narrow and broad atomic layers, respectively), with a relative ordering consistent with the analysis deduced from the DOS curves in Fig. 4. Let us emphasize that the beat location depends on the width of the atomic layers.

As was inferred from our previous investigations on the influence of the softness of the potential profile,[16] most of the information about the effective potential experienced by the valence electrons, deduced from the set of magic numbers, are actually provided by the beat locations. The strength of the shell closing effects, linked to the KS level gaps, also provides valuable information.

This contrasts with the fundamental size period $\Delta N_e \approx 0.6$, which seems universal for any spherical potential box involving narrow surface wall and flat average bottom. In the present case this quasiperfect agreement with the JBM is particularly striking, and was not expected, owing to the large amplitude of the effective potential distortions.

Calculations involving damped potential oscillations in the central region of the cluster have been performed to artificially wipe out eventual spurious effect due to frequent unphysical innermost layer location [Figs. 5(c) and 6, curve *c*]. By comparing curves *b* and *c* of Fig. 6, we see that the radial region close to the cluster center has no effect on the electronic shell structure; this supports what was stated in previous sections. Invoking a progressive destruction of the multiple-shell geometry inside the cluster by temperature effects, leading to a homogeneous inner density, we have carried out model calculations with oscillating cusp patterns which are damped from the first outer spherical layers [Figs. 5(d) and 5(f)]. Such potentials can be qualitatively reproduced by assuming a progressive increase of the ionic layer width in the inner cluster region. These potential profiles, which are consistent with the surface ordering obtained in liquid metal-vapor interface calculations,[56] lead to electronic shell structures which are practically identical to those obtained by assuming development of the multiple-shell structure over the whole cluster volume (see Figs. 6, curves *d* and *f*), at least in the size range studied. We have noted changes in the supershell structure only for a very narrow extent of the modulation. Actually, by assuming the semiclassical approach, it is clear that the occurrence of a supershell pattern shift is undoubtedly correlated with the relative proportion of flat and oscillating radial potential regions which are probed by closed triangular and square classical orbits. All our results point out the central part of the surface properties and

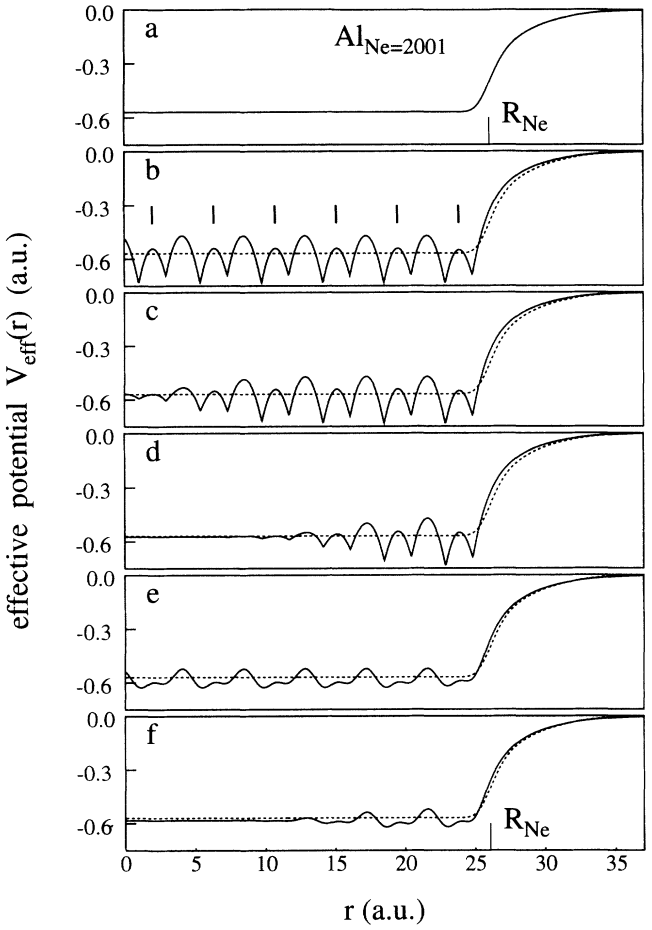

FIG. 5. Electronic effective potentials, fitted on self-consistent results, used in independent-electron calculations for aluminum clusters. The corresponding shell-correction energy curves are plotted in Fig. 6. Empty-core parametrization of the electron-ion interaction is assumed ($r_c = 0.97$ a.u.). (a) JBM-like effective potential. (b) Effective potential for a multiple-shell structure involving zero-width ionic layers. (c) Same as (b) except for the damping of the innermost potential oscillations. (d) Effective potential for a damped multiple-shell structure extending over only the three outermost ionic layers. (e) Effective potential of a multiple-shell structure involving broad ionic layers (a truncated Gaussian radial ion distribution having a FWHM equal to $0.3d$, where d is the layer spacing). (f) Effective potential for a damped multiple-shell structure with broad ionic layers extending over only the three outermost ionic layers.

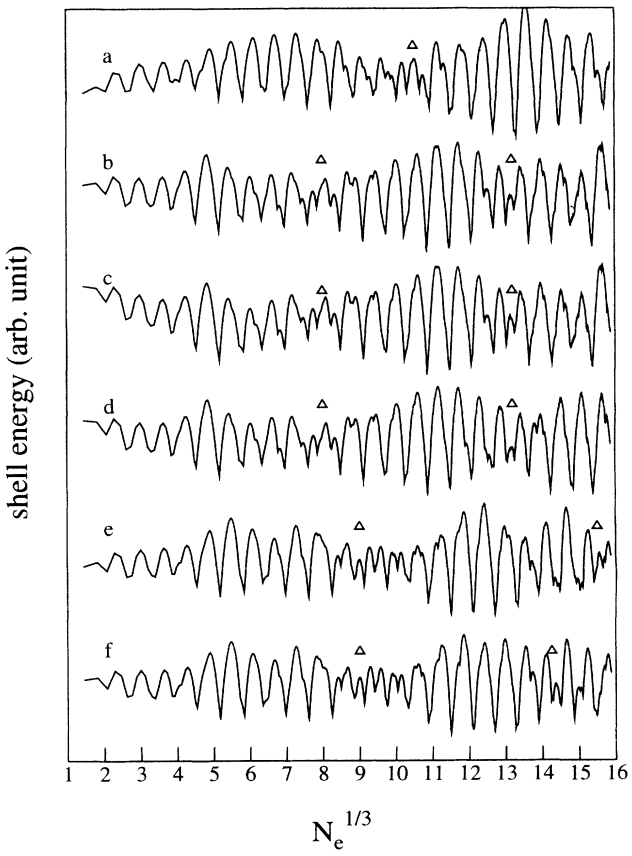

FIG. 6. Shell-correction energy curves corresponding to the electronic effective potentials plotted in Fig. 5. The major magic sizes correspond to the sharp minima. Approximate locations of the beat regions are indicated by triangles. Roughly, in a given size domain, all these oscillating curves are relatively π or 2π shifted, depending on the relative location of their respective beat patterns.

ionic arrangements in the development of the electronic shell structure.

C. Influence of the ion-pseudopotential parametrization

In this section we report some calculations illustrating the dependence of the electronic shell structure on the effective pseudopotential which is assumed to describe the electron-ion interaction. This study is not purely academic: this sensitivity has to be kept in mind in all *non-ab-initio* granular models, involving inhomogeneous ionic distributions or/and particular parametrization of the ion pseudopotential. The best choice in mesoscopic systems is far from being definitively assessed, and numerous approaches, derived either from atomic or from condensed-matter physics, are found in the literature.[58-60,65-69]. If some properties are quite insensitive to the accuracy of the pseudopotential, as the electronic shell structure in the small-size domain, we stress that this is not the case for the supershell structure. This will be shown clearly below.

For instance, assuming an empty-core parametrization, the radius r_c depends on the bulk or atomic physical properties used in the fitting procedure (see Table I). As a drastic example, the effective r_c value for lithium is 1.75 or 1.06 a.u. when requiring matching of either the atomic ionization potential or bulk metal properties,[58-60] respectively. Differences are smaller in the case of aluminum (0.97 and 1.12 a.u.) or sodium (1.74 and 1.67 a.u.). The noticeable influence of the ion-core volume on the supershell structure is expected from Sec. IV B since the node locations are found to depend crucially on the exact profile of the spherically averaged pseudopotential: a change in the r_c value modifies the relative width and height of the bumps corresponding to the ionic-shell and intershell regions. Sophisticated pseudopotentials, referred to as "norm-conserving," constructed from full-core *ab initio* atomic calculations, are available.[67,69] However, a strict application of these refined pseudopotentials, which are nonlocal (a specific pseudopotential is defined for each angular momentum—relative to the ionic core—of the valence states), would lead to a formidable numerical complexity for large clusters. Forsaking the SAPS approximation, the introduction of a basis set of atomic pseudo-wave-functions, centered around each ionic site, is necessary in order to preserve the full advantages of these refined pseudopotentials.[32] Restoring the standard and practical approximations (locality and SAPS approximation) requires selecting a pseudopotential corresponding to a specific l-valence state. As discussed by Blundell and Guet,[61] this approximation is severe in the case of lithium, which contains s-core states only, and introduction of the neglected p component of the pseudopotential would probably correct the overestimated effective core radius (the same as for sodium) and thus the overestimated cluster volume obtained from the microscopic SAPS calculations. In fact we believe that a simple local parametrization fitted on bulk properties, as done originally by Ashcroft with the single-parameter empty-core profile,[58] is a reasonable compromise which simultaneously allows us to avoid the explicit introduction of the l dependence (equivalent to some suitable weighted average of the l-dependent pseudopotentials) and eliminates eventual problems of transferability which could occur in using atomic pseudopotentials in a bulk metal environment. This could explain the efficiency of these empirical pseudopotentials in the study of metal surface properties,[53] although they are not theoretically derived from first principles as are the norm-conserving ones. Nevertheless we emphasize that all results reported in this paper are qualitatively independent of the exact pseudopotential profile inside the ionic core. All trends concerning the electronic shell structure changes depend on the essential ingredient of finite core-volume granular models: the electron-ion interaction at short distances is more repulsive than the Coulomb law involved in electrostatic models such as the structureless JBM. In comparison with Ashcroft empty-core parametrization, norm-conserving pseudopotentials are softer near r_c and present either a repulsive positive bump or a soft attractive well over the ionic volume. In this section we give only trends which are expected for the supershell shifts if more attractive or repulsive ion pseudopotentials, relative to the zero value of the usual Ashcroft parametrization, are assumed inside the ion core. For this purpose we present in Figs. 7(a), 7(b), and 8, curves a and b, results obtained for aluminum with a constant pseudopotential value inside the ion core, namely $A=1.8$ a.u. (repulsive case) and $A=-Z_v/r_c\approx-3.1$ a.u. (attractive case). These values are chosen arbitrarily. In the case of aluminum, the s-valence-state norm-conserving pseudopotential exhibits a soft bump culminating at 1.6 a.u. at the center, while p-valence-state ones are rather flat around the value -1.6 a.u.[69] Construction of the electronic effective potentials and shell-energy calculations are carried out within the same procedure as described in Sec. IV B.

For all pseudopotential parametrizations the size-shell spacing is found to be very close to the JBM one. In the case of more repulsive electron-core interaction [curves Figs. 7(a) and 8(a)] the electronic shell structure is close to the JBM predictions (curve of index 0 in Fig. 8), except for some details in the beat region and slight shifts of the magic numbers. The agreement is much better than the one observed with the usual Ashcroft prescription ($A=0$) inside the ionic core [in Figs. 5(e) and 6, curve e], although the amplitude of the pseudopotential modulation is of the same order of magnitude in both cases. Two main profile features are relevant to the magnitude of the electronic structure change: (i) the phase of the modulation at the outermost ionic shell (dip or bump); and (ii) the amplitude of the d-period Fourier component of the periodic radial potential. The modulation of the curve in Fig. 7(a) is dominated by the harmonic component of period $d/2$ and therefore has a much weaker influence on the electronic shell structure (the aluminum Fermi wavelength is equal to 6.8 a.u.). In the case of more attractive electron-core interaction, the almost perfect sinelike modulation has a large amplitude and results in a considerable change in the supershell pattern [Figs. 7(b) and 8, curve b].

The curves of Figs. 7(c), 7(d), and 8 (curves c and d) are

results obtained with phenomenological effective potentials built by adding an exponentially damped d-period sine curve to the optimized JBM-like phenomenological potential profile (dashed curves in Fig. 7) below R_{N_e}. A shift of the beat location to lower or higher sizes, relatively to the JBM result, can be produced by a simple $\pi/2$-phase shift of the sine curve (equivalent to a change of the location of the outer ionic layer equal to $d/4 \approx 1.1$ a.u.) Comparison of curves of Figs. 7(b)–7(d) and 8 (curves b–d) shows that the relative location of the first ionic layer and of the potential wall is the most crucial parameter. This study points out that accurate self-consistent quantum calculation of the shape of the surface potential is highly required to predict correctly the electronic shell structure in the large-size domain.

D. Liquid-cluster model

When the temperature is high enough, as compared to the melting point of the cluster, stable geometrical structures (bulklike or multiple-shell) are unable to develop, and large scale inhomogeneities in the inner ionic distribution are expected to vanish. If a homogeneous ion-location distribution is assumed over the entire cluster volume, its spherically averaged component is flat in the radial domain $0 < r < R_{N_e}$, and does not exhibit noticeable radial modulation, contrary to the case of multiple-shell structures. Strictly speaking, the instantaneous radial distribution is actually a series of very close Dirac functions. However, the resulting total pseudopotential is a smooth function [for illustration see Fig. 1, and remember that only the difference $V^{ps}(r) - V^{jel}(r)$ is displayed] with a completely negligible residual high-frequency modulation, reminiscent of the granular structure. Hence the pseudopotential $V^{ps}(r)$ can be calculated by assuming a *continuous* homogeneous ion distribution in the sphere of radius R_{N_e}. This fairly good numerical approximation does not need to involve time averaging. The exact choice for the radius of the distribution has no influence on the electronic shell structure. In previous sections, total pseudopotentials from broad ionic layers were calculated by taking N_j-normalized *continuous* distributions $f(R - R_j)$ [see Eq. (3)]. A more refined model would involve a softer ion-density profile at the surface to take into account the surface corrugation. The liquid-drop model investigated in this section is actually almost identical to the conventional electrostatic JBM: the single difference is that a more appropriate electron-ion in-

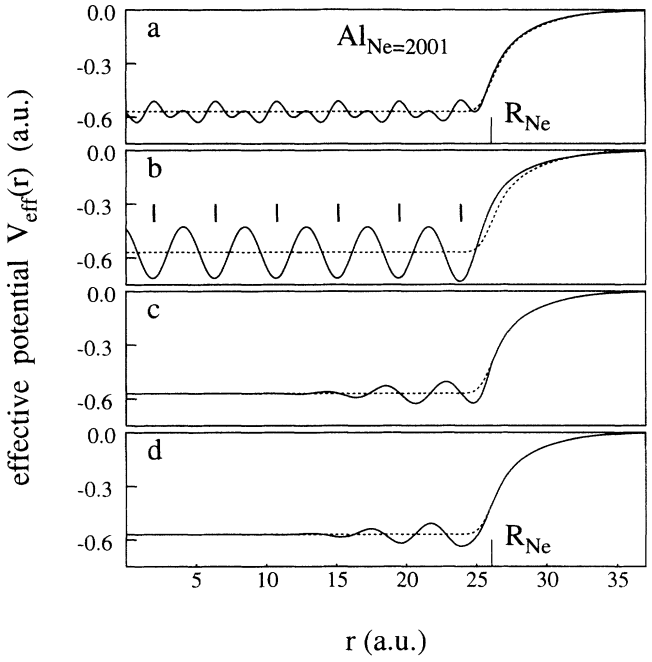

FIG. 7. Electronic effective potentials, fitted on self-consistent results, used in independent-electron calculations, for aluminum clusters. The corresponding shell-correction energy curves are plotted in Fig. 8. An empty-core parametrization of the electron-ion interaction, with $A \neq 0$ [see Eq. (2)], is assumed ($r_c = 0.97$ a.u.). (a) Effective potential for a multiple-shell structure involving broad ionic layers (a truncated Gaussian radial ion distribution having a FWHM equal to $0.3d$, where d is the layer spacing), and for $A = 1.8$ a.u. (b) Same as (a), except $A = -3.09$ a.u. The locations of the ionic layers are indicated by short vertical lines. (c) and (d) Phenomenological potentials built by adding an exponentially damped d-period sine curve to the phenomenological JBM-like potential (dashed curves in all the figures). In (c) the outermost minimum is located at $R_{N_e} - d/4$; in (d) the outermost minimum is located at $R_{N_e} - d/2$ (a sine curve of period $2d$ is used to smoothly connect this minimum to the JBM potential wall).

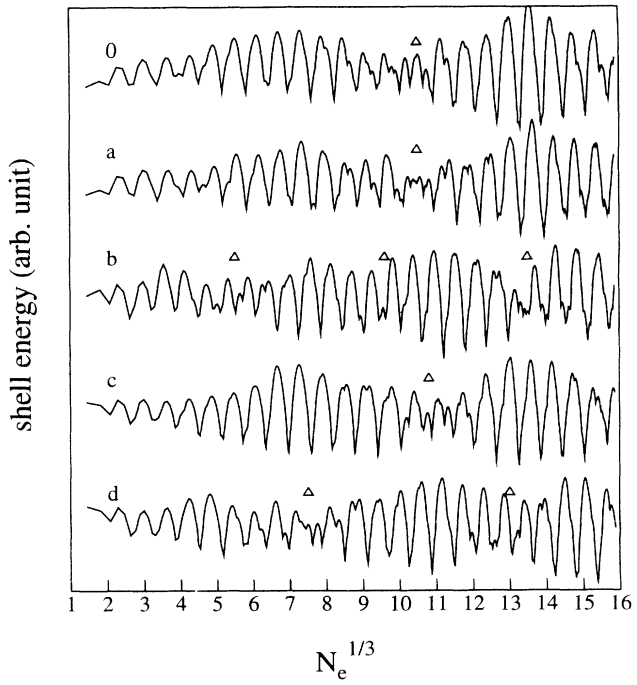

FIG. 8. Shell-correction energy curves corresponding to the electronic effective potentials plotted in Fig. 7 (the curve of index 0 is the JBM result). The major magic sizes correspond to the sharp minima. Approximate locations of the beat regions are indicated by triangles. Roughly, in a given size domain, all these oscillating curves are relatively π or 2π shifted, depending on the relative location of their respective beat patterns.

teraction is substituted for the Coulomb law inside the ionic cores. The total electron-ion pseudopotential is then expressed as

$$V^{ps}(r)=\int_0^{R_{N_e}} 4\pi \left[\frac{n_0}{Z_v}\right] v^{ps}(r,R)R^2 dR \ . \quad (4)$$

Instead of displaying $V^{ps}(r)$, more insight into the specific features introduced by including a more suitable electron-ion interaction is provided by calculating the positive charge density of the underlying equivalent electrostatic model, with the help of the Poisson equation. Note that the empty-core pseudopotential of a single ion cannot be derived from any charge distribution (except in the specific case $A=-Z_v/r_c$) contrary to its spherical average $V^{ps}(r,R)$ [Eq. (2)]. For instance, for $A=0$, the associated charge density consists of two spherical δ functions peaked at $R-r_c$ and $R+r_c$, containing the charges $Z_v(R-r_c)/2R$ and $Z_v(R+r_c)/2R$, respectively. The equivalent charge distributions are plotted in Fig. 9. Taking into account the electron-ion interaction through Ashcroft empty-core formula introduces an effective stairlike surface inhomogeneity in the ionic background density. The additional step extends over the radial domain $R_{N_e}-r_c<r<R_{N_e}+r_c$, and analytical evaluation leads to the formula

$$n_+(r)=\frac{n_0}{2}\left[1-\frac{r_c}{r}\right] \quad (5)$$

[while $n_+(r)=n_0$ for $r<R_{N_e}-r_c$]. For large clusters, the size evolution of this quasi-step-profile is imperceptible. The change in the equivalent positive charge density, relative to the simple JBM square shape, depends on the parametrization of the ion pseudopotential. A steep triangular spike is obtained for more repulsive electron-core interaction [$A=1.8$ a.u. in Eq. (2)]. Let us emphasize that the jellium is encountered by the valence electrons through its electrostatic potential, which partially erases the jellium shape differences, and, in particular, hard walls are smoothed. In consequence this narrow skin of weaker density is expected to act as a smooth jellium and to yield a KS effective potential softer than the JBM one. Note that such a stairlike surface profile was recently assumed (in a purely phenomenological model) by Mansikka-aho, Manninen, and Nishioka to simulate the covering of aluminum clusters by an alkali atomic layer.[70] These authors suggested producing such mixed clusters in order to study experimentally the effects of surface softness.

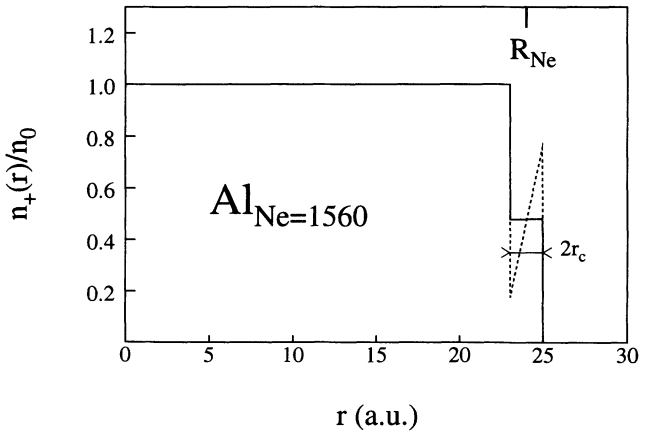

FIG. 9. Equivalent jellium density, normalized to the bulk mean value, corresponding to the liquid-cluster model. This model involves a homogeneous spherical ionic distribution and an empty-core parametrization of the electron-ion interaction [see Eq. (2)]. The overall effect of the non-Coulombic electron-ion interaction over the ionic cores ($r_c=0.97$ a.u.) is equivalent to the effect produced by a jellium skin of weaker average density, extending over the radial region ($R_{N_e}-r_c$, $R_{N_e}+r_c$). Solid and dashed curves correspond to the values $A=0$ and 1.8 a.u., respectively [see Eq. (2)].

1. *Results for trivalent species*

In Fig. 10 are plotted typical results of self-consistent KS calculations for various cluster sizes, and for the same pseudopotential parametrizations as in Fig. 9. As expected, the surface profiles of the electronic potential wells are softer than the JBM one, and the increase of the softness is correlated to the increase of the repulsive character of the electron-ion interaction. As in the JBM and multiple-shell cluster models, which both involve the same surface description of the ionic background for each size, the surface potential profile is quasi-size-independent and can be parametrized according to a functional form $\mathcal{V}(r-R_{N_e})$.

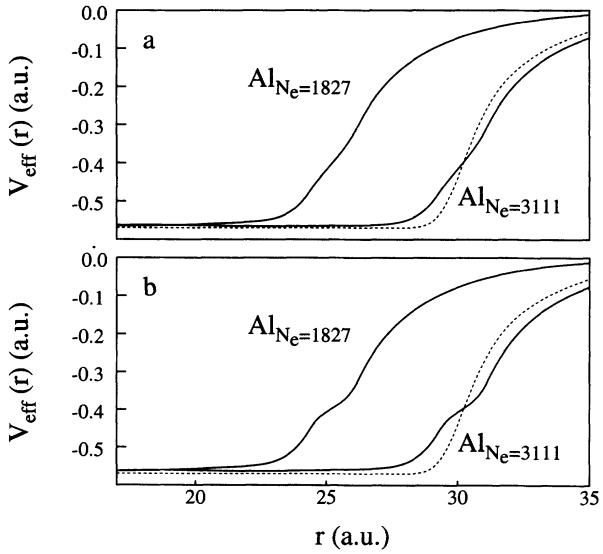

FIG. 10. Typical self-consistent Kohn-Sham effective potentials obtained in the liquid-cluster model, for aluminum clusters. The dashed curves correspond to the phenomenological JBM-like potential. The equivalent jellium densities are plotted in Fig. 9. Empty-core parametrization [see Eq. (2)] of the electron-ion interaction is assumed. (a) $r_c=0.97$ a.u., $A=0$ a.u. (b) $r_c=0.97$ a.u., $A=1.8$ a.u. (strongly repulsive electron-ion interaction inside the core).

As before, we have applied the reliable method of Refs. 62 and 64 to calculate the size-shell structure for spherical liquid clusters and the empty-core parametrization of the electron-ion interaction. The size-independent "phenomenological" surface potentials, fitted on self-consistent results, and the corresponding shell-correction energy curves, are plotted in Figs. 11 and 12, respectively. The phenomenological JBM potential profile (dashed curves in Fig. 11) leads to a shell structure (curve of index 0 in Fig. 12) in very good agreement with complete size-to-size self-consistent calculations.[13,62] The supershell beat is located around $N_e^{1/3}=10.5$ ($N_e=1150$). As expected from Ref. 16 the effective surface softness arising from the non-Coulombic interaction inside the ionic cores leads to a large shift of the beat location [$N_e=2000$ for Fig. 12(b)]. Comparison of the various results points out that the predicted supershell structure depends crucially on the electron-ion interaction, but the trend (shift of the first beat toward higher sizes, all the more as the softness is larger) is a systematic feature of soft potentials. Besides the influence of the strength of the repulsive interaction (compare curves *a* and *b* in Fig. 12) the exact extent of the non-Coulombic region is suspected to be of particular importance for determining the shell structure, especially for low-r_s metals. The potential profile of Fig. 11(c) is obtained with the value $r_c=1.12$ a.u. deduced by Ashcroft[58] to reproduce bulk aluminum properties. The change in the r_c-value is small (0.15 a.u.) but noticeable increase of the surface softness and shift of the beat size domain are observed (compare curves *a* and *c* in Fig. 12).

We have carried out the same investigations for gallium clusters. The r_c parameter was fixed to the value minimizing the r_s-dependent bulk energy functional (with the electrostatic interaction appropriate to liquid structure) at the observed experimental density (see Table I). The matching of the ionization potentials (IP's) of the valence shell would lead to practically the same core radius as aluminum (the first IP differs by less than 1% and the two others by roughly 7%). This value is identical to the tabulated ionic radius of Ga^{3+} in crystal. For the purpose of consistency with the other metals studied, we checked that the r_c values taken from the condensed-matter physics literature for aluminum and alkali species (see below) are close to the ionic radius and the empty-core radius, ensuring the bulk stability at the actual r_s value (see Table I). Results for the electronic supershell pattern are shown in Fig. 13. As for aluminum the beat pattern is shifted toward higher sizes (curve *b* of Fig. 13) relative to the JBM prediction (curve *a* of Fig. 13). Increase of the repulsive interaction inside the core volume, as exhibited by norm-conserving pseudopotentials for *s*-valence states for trivalent s^2p metals, could bring the location of the supershell beat closer to the experimental result. Nevertheless, if the standard Ashcroft parametrization ($A=0$) is assumed, agreement with the experimental result [beat around $N_e=2500$ (Ref. 25)] could be

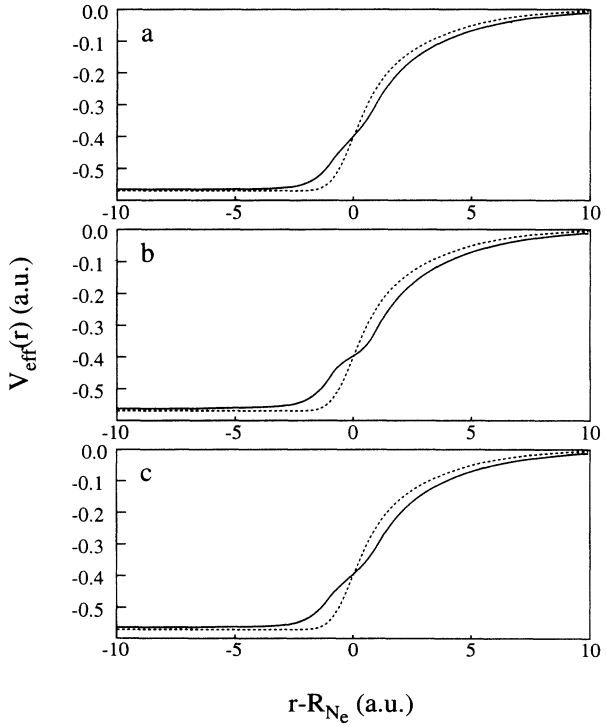

FIG. 11. Electronic effective potentials, fitted on self-consistent results, used in independent-electron calculations, for aluminum clusters. The corresponding shell-correction energy curves are plotted in Fig. 12. The dashed curve is the phenomenological JBM-like potential. Empty-core parametrization of the electron-ion interaction is assumed [see Eq. (2)]. Curve *a*, $r_c=0.97$ a.u., $A=0$ a.u. Curve *b*, $r_c=0.97$ a.u., $A=1.8$ a.u. Curve *c*, $r_c=1.12$ a.u., $A=0$ a.u.

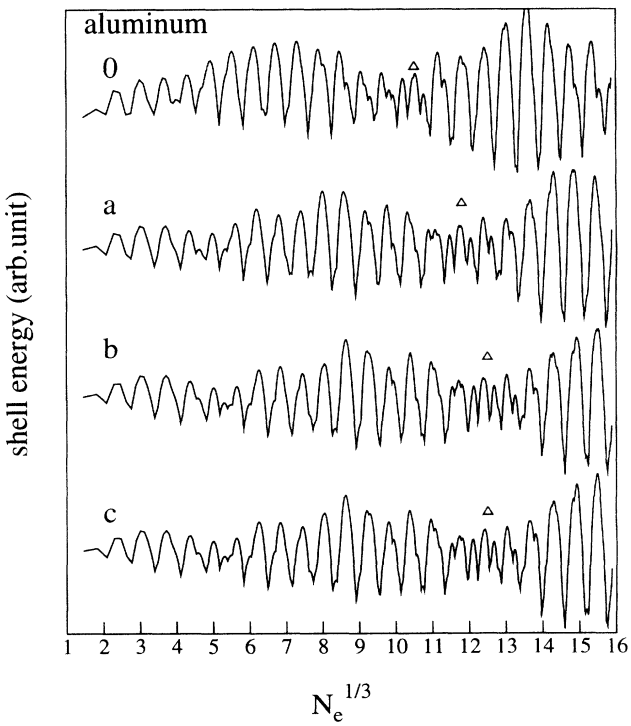

FIG. 12. Shell-correction energy curves corresponding to the effective potentials plotted in Fig. 11 (the curve of index 0 is the JBM result). Approximate locations of the beat regions are indicated by triangles.

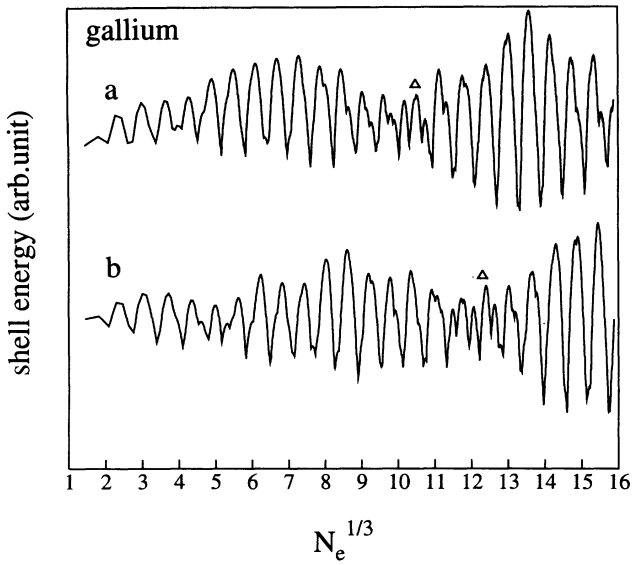

FIG. 13. Shell-correction energy curves for gallium clusters obtained in the liquid-cluster model. Empty-core parametrization of the electron-ion interaction is assumed: $r_c = 1.17$ a.u. and $A = 0$ in Eq. (2). Curve *a*, results obtained with the phenomenological JBM-like potential. Curve *b*, results obtained in the liquid-cluster model.

achieved by relaxing the arbitrary step profile of the surface ion distribution. For instance, a spherical average of the eventual surface roughness would lead to a soft ionic distribution at the surface. In order to compare our results with Ref. 25, we have assumed the same density profile: the shape is triangular over a thickness ε (the overall ion density is trapezoidal). Calculation shows that a thickness ε on the order of 3 a.u. (value scarcely larger than the diameter of Ga^{3+}) is sufficient to reproduce the experimental beat location. Note that this value is noticeably lower than the one required within the diffuse JBM of Ref. 25 ($\varepsilon = 6$ a.u.).

Stating that the supershell pattern shift could be induced by eventual surface roughness does not question the reliability of our calculations involving a corrugated spherical hard-walled potential box, which give rise essentially to a weakening of the shell structure (see Sec. II B). Actually, from our experience of the effects of surface softness,[16] we know that a noticeable shift of the supershell pattern occurs only beyond some critical softness threshold, which depends on the r_s value. Thus, as far as hard-walled potentials and weak corrugations are involved, the effective softness (obtained by spherically averaging the surface roughness) is too weak to induce a large change of the shell structure. In that case, the single effect of the surface roughness is the breakdown of the perfect spherical symmetry which leads to a damping of the shell effects. On the other hand, when the same roughness is added to a soft effective potential, its impact on the supershell pattern is magnified.

2. *Results for alkali species*

In the case of alkali metals, which are characterized by large-r_s values, changes induced by a given increase of the surface softness will be smaller, as compared to trivalent metals. Since the expected beat shift will be tiny on a $N_e^{1/3}$ scale, and the magic sizes depend little on the potential surface shape, systematic rules for defining the beat region have to be substituted for a simple eye inspection of theoretical plots or experimental spectra. The beat region is characterized by a weaker amplitude of the shell effects and enhancement of the subshell structures. This last feature is theoretically reflected through a frequency doubling of the pattern on an $N_e^{1/3}$ scale. Experimentally the subshell-related features are often obscured by thermal effects and the breaking of perfect spherical symmetry (see Sec. II B). As far as theoretical calculations are concerned, a complete self-consistent procedure leads to subshell structures smoother than those obtained within the independent-electron approach.[62] The best method, systematically used in most papers, consists of plotting the cube root of the successive major magic numbers N_e against a running integer index.[8–11,25] The points lie on two straight lines which are shifted by one-half size-shell period at the beat region. Following this approach, we will characterize the extent of the beat size domain by the highest (lowest) clear magic size spaced from the previous (following) ones by the standard size shell spacing $\Delta N_e^{1/3} \approx 0.6$.

In Fig. 14 electronic surface densities and potentials obtained within the liquid-cluster model are drawn and compared with JBM results. An increase of the softness leads to a reduction of the main Friedel oscillation, which

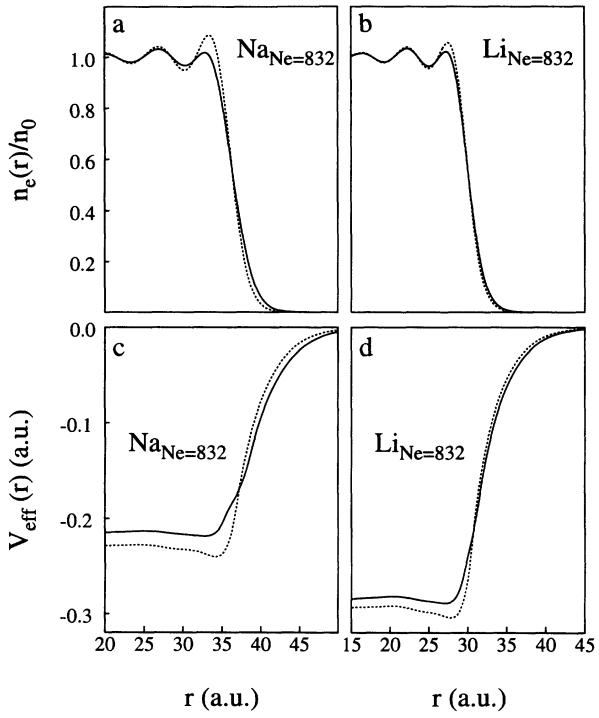

FIG. 14. Self-consistent electronic density (upper figures) and Kohn-Sham effective potential (lower figures) obtained for sodium and lithium in the liquid-cluster model. The dashed curves are the JBM results. Ashcroft empty-core parametrization of the electron-ion interaction is assumed; sodium clusters: $r_c = 1.67$ a.u.; lithium clusters: $r_c = 1.06$ a.u.

is a systematic feature of low-density metals.[53] The energy shift of the potential bottom results essentially from the change in the electrostatic dipole barrier. The resulting increase of the Fermi level gives rise to a decrease of the ionization potentials, and thus a better average agreement with experiment.[2] The r_c values are taken from Ref. 59: $r_c=1.67$ and 1.06 a.u. for sodium and lithium, respectively.

Shell-correction energy curves for sodium and lithium (curves *a* and *c* in Fig. 15, respectively) from independent-electron calculations involving JBM-like potential surface profiles are in very good agreement with self-consistent results reported by Genzken and coworkers.[12,13] For sodium the major difference is an enhancement of the subshell structure near $N_e^{1/3}=8.5$, which enlarges the frequency-doubled pattern on the small-size side. This feature can also be noticed in the paper by Clemenger.[64] In any case, in curve *a* of Fig. 15 or in Refs. 12 and 13, the magic size $N_e=912$ is clearly the first magic number of the series associated with the second antinode region. In the experimental spectrum displayed in Ref. 9 this size lies manifestly close after the *beginning* of the beat pattern, and can be related to a noticeable subshell structure enclosed by the dips estimated at $N_e=800$ and 970. Because of the lower signal-to-noise ratio in the large cluster domain, determination of the location of the dips after the beat by simple eye inspection is imprecise (particularly in the size range $N_e=1600-1800$), but a strong regular oscillation grows from $N_e=1120$ and all the dip locations indicated by the authors (1120, 1310, 1500, . . .) are close to the JBM results. The beat shift is clearly exhibited in the paper by Genzken[13] where both theoretical and experimental results are juxtaposed. Curve *b* in Fig. 15 is the result of the liquid-cluster model. The beat region is found to be located between $N_e=832$ (last noticeable subshell-related size in the beat pattern of the JBM) and 1100, in good agreement with experiment. We recall that in Ref. 9 the spectra involve warm sodium clusters. Calculations with $r_c=1.74$ a.u. lead to identical results. With regard to the low shell closing numbers, this model also corrects some insufficiency of the JBM. The JBM predicts magic sizes at $N_e=34$, 186, and 254,[13] when the experimental magic sizes, clearly assigned in this size domain, are $N_e=40$, 198, and 264.[9] The liquid-cluster model leads to the values 40, 198, and 254/268 (see Fig. 15).

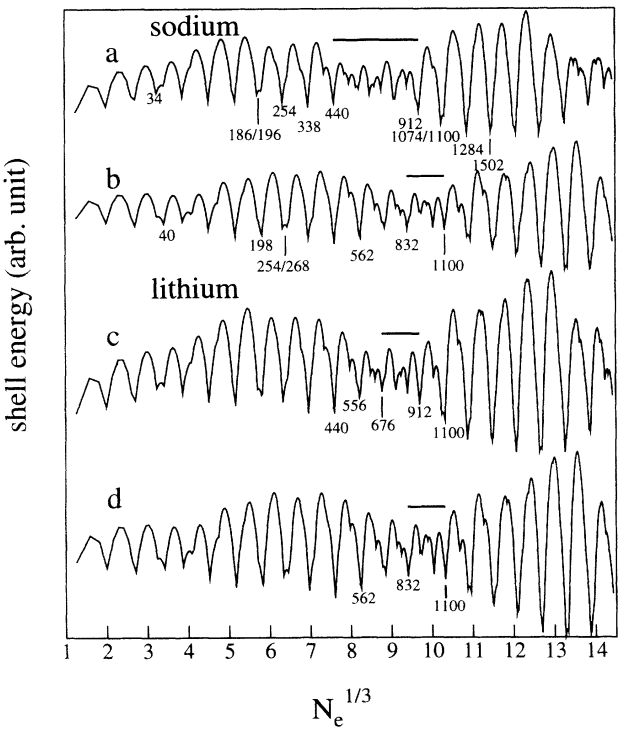

FIG. 15. Shell-correction energy curves obtained from independent-electron calculations involving phenomenological effective potentials fitted on self-consistent results. Curve *a*, JBM results for sodium. Curve *b*, results obtained in the liquid-clusters model ($r_c=1.67$ a.u.). Curve *c*, JBM results for lithium. Curve *d*, results obtained in the liquid-cluster model ($r_c=1.06$ a.u.). Extents of the beat patterns, defined according to the procedure described in Sec. IV, are indicated by short horizontal lines.

Curve *c*, Fig. 15, displays the JBM shell-correction energy obtained for lithium. These results are practically identical to those derived from complete self-consistent JBM calculations, even in the beat region ($N_e=676-912$).[13] Obviously the exact amplitude is not correctly reproduced since in the independent-electron approach the shell energy is merely extracted from the sum of the N_e lowest electronic states. Evidence for the supershell structure in lithium clusters was recently reported by Brechignac *et al.*[11] If only the listed shell closing numbers observed at high temperature are considered, the experimental beat is bounded by the cluster sizes $N_e=820$ and 1065. Let us emphasize that the minor magic numbers, related to subshell structures and observed at low temperature, have to be disregarded to define accurately the beat location. The reason is that these sizes are linked by the standard size spacing $\Delta N_e^{1/3}\approx 0.6$ to the lower or upper series of strongest shell closing numbers, and thus they lead to an arbitrary choice for the selected sizes defining the onset and the end of the beat domain. For instance, in curve *a* of Fig. 15 (sodium case), the overestimated strength of the frequency-doubled pattern enlarges the beat region and its location is defined less accurately. Our model calculation (curve *d*, Fig. 15) leads to a beat domain clearly enclosed by the magic sizes $N_e=832$ and 1100 (as for sodium), in close agreement with experiment. Note that, although the potential softness for lithium is smaller than for sodium, its effect is slightly magnified by the lower r_s value. Calculations with the value $r_c=1.75$ a.u. (matching of the atomic ionization potential) leads to a beat region enclosed by the magic sizes $N_e=1218$ and 1556. This location is manifestly too high as compared with experiment, indicating that the *p* component cannot be disregarded for lithium when using norm-conserving nonlocal pseudopotential, as it was pointed out by Blundell and Guet[61] and also noted by Blaise *et al.*[38] from *ab initio* calculations. Owing to the $1s^2$ ionic configuration, the Pauli-exclusion principle does not apply for *p* states

which are allowed to penetrate the ionic volume. The related p pseudopotential is thus more attractive than the pseudopotential appropriate to s-valence states. This is roughly equivalent to reducing the effective core radius r_c in the Ashcroft parametrization. With the parameters listed in Ref. 69, we have found that the p-pseudopotential well is very deep [minimum $V(r) \approx -2$ a.u. at $r \approx 0.5$ a.u.].

As in the case of the conventional JBM the theoretical large magic sizes are not exactly those reported in the experimental works. This is not surprising, owing to the simplicity of the models, and to the experimental uncertainty in determining the closing numbers in noisy or weakly contrasted mass spectra. In any case, taking into account the effective jellium softness induced by the repulsive part of the electron-ion interaction brings theory and experiment into better agreement.

V. CONCLUDING REMARKS

In this paper, the electronic shell structure for spherical multiple-shell clusters has been investigated in the large-size domain. Complete self-consistency was not attempted as in microscopic calculations using the SAPS technique. However, our results are derived from reliable approximations and the critical ingredient, namely the electronic potential profile at the surface, has been determined self-consistently. This study shows that the JBM-like electronic shell structure, characterized by the shell-size spacing $\Delta N_e^{1/3} \approx 0.6$, develops systematically in spite of the strong inhomogeneity in the ionic distribution. In particular the magic sizes in the small-size domain do not differ from JBM predictions. In contrast, the supershell pattern depends crucially on the width of the ionic layers (changes induced by thermal effects, for instance), and on the exact parametrization of the ion pseudopotential. In addition, it was proved that only the structure of the outermost layers is relevant. For all the ionic structures reported in this paper, the beat location is shifted toward lower sizes, as compared to the JBM results, in contradiction with experiment. Presently there is no experimental evidence for the multiple-shell structure except in the specific case of carbon clusters undergoing an intense electron bombardment.[71] However, if perfect spherical symmetry is assumed, such ionic layering at the surface is not irrelevant. Nevertheless this speculative structure, numerically practical, is useful to test the influence of finite core-volume and density inhomogeneities on the electronic shell structure. We believe that the results can be generalized to any ionic structure, ensuring approximately the spherical symmetry and a constant average density on a large scale: (i) The shell periodicity $\Delta N_e^{1/3} \approx 0.6$ and the clear emergence of the electronic shell structure in actual granular clusters result from the overall shape only, and not from statistical averaging. (ii) The supershell structure depends strongly on the ionic distribution at the surface. These features could explain why the supershell pattern for aluminum clusters, a trivalent metal of high melting point, was not clearly observed: an increase of the source temperature favors the spherical shape, but the ions tend continually to organize themselves to form facets and fcc bulklike seeds.

The predictions of the liquid-cluster model, which involves a homogeneous ionic distribution, are consistent with the electronic shell structures observed for the low melting point metal clusters (in fact homogeneity over a small radial region below R_{N_e} probably would lead to the same predictions). In the case of a homogeneous ion density the effects of the non-Coulomb electron-ion interaction over the core volume are concentrated at the surface and are reflected through an effective increase of the electronic potential softness, equivalent to a diffuse jellium. This additional softness induces a beat shift toward higher sizes, as compared to the JBM results. Assuming simple Ashcroft empty-core parametrizations of the ion pseudopotentials, the beat locations for sodium and lithium are found to be close to experimental values. For gallium the model predicts a beat location around $N_e \approx 1800$, below the experimental value $N_e \approx 2500$. Calculations involving a more accurate pseudopotential are necessary to estimate the respective influences of the electron-ion interaction and surface softness of the ion distribution.

At the end of the writing of this paper, we became aware of recent works by Reinhard *et al.*[72] and Genzken *et al.*,[73] in which the jellium diffuseness (assumed in Refs. 47–50) is related to the finite ion-core volume, and a paper by Serra *et al.*,[74] who use a model closely related to our liquid-cluster model to investigate the optical response of lithium clusters. These last authors use the local velocity-dependent pseudopotential introduced by Bachelet, Ceperley, and Chiochetti.[68] Taking into account only the s and p valence states, Bachelet, Ceperley, and Chiochetti expressed the non-local norm-conserving ion-pseudopotential of Hamman, Schlüter, and Chiang[67] in a local form, cast as the sum of two velocity-dependent terms and a potential term. The spherical average in Eq. (4) leads to a total pseudopotential having the same form, except that the electronic dynamic variables and operators are now defined relative to the cluster center. It would be very fruitful to investigate the electronic shell structure of simple metal clusters with this refined pseudopotential. Contrary to our local approach, in which most of the effects arising from the electron-ion interaction can be analyzed in terms of surface softness, velocity-dependent pseudopotentials simultaneously involve concepts of different nature, for instance an r-dependent effective mass. With regard to the supershell pattern, the equivalence of both approaches is far from being obvious. The vanishing of the velocity-dependent terms and the Coulombic behavior of the potential one occur beyond $r_c \approx 3.5$ a.u. for lithium. If we ignore the two kinetic terms, the potential term alone undoubtedly gives rise to a softness larger than the one displayed in Fig. 14 (obtained with $r_c = 1.06$ a.u.) An effective decrease of the surface smoothness to bring about the beat at the experimental location is thus necessarily ensured by the two velocity-dependent terms. This leads to a rather complicated interpretation of the theoretical results, as compared to a local approach. At the price of a loss of accuracy, the advantage of a local formalism is to allow straightforward predictions. For example, a softness increase of the potential surface profile enlarges the

effective cluster radius R or, equivalently, the electron spillout. This picture qualitatively explains the discrepancies between the JBM theoretical and experimental static polarizabilities and plasmon frequencies from simple reference to their classical counterparts, which scale as R^3 and $(N_e/R^3)^{1/2}$, respectively. In a future paper, we will report our model calculations involving spherical potential wells with surface roughness.

ACKNOWLEDGMENTS

We are very grateful to C. Guet for stimulating discussions about pseudopotential concepts. The Laboratoire de Spectrométrie Ionique et Moléculaire is "Unité Associée au Centre National de la Recherche Scientifique N°171".

[1]W. D. Knight, K. Clemenger, W. A. de Heer, W. A. Saunders, M. Y. Chou, and M. L. Cohen, Phys. Rev. Lett. **52**, 2141 (1984).
[2]W. A. de Heer, Rev. Mod. Phys. **65**, 611 (1993).
[3]M. Brack, Rev. Mod. Phys. **65**, 677 (1993).
[4]W. Ekardt, Phys. Rev. B **29**, 1558 (1984).
[5]D. E. Beck, Solid State Commun. **49**, 381 (1984).
[6]W. Kohn and L. J. Sham, Phys. Rev. **140**, 1133A (1965).
[7]R. Balian and C. Bloch, Ann. Phys. **69**, 76 (1972).
[8]H. Nishioka, K. Hansen, and B. R. Mottelson, Phys. Rev. B **42**, 9377 (1990).
[9]J. Pedersen, S. Bjørnholm, J. Borgreen, K. Hansen, T. P. Martin, and H. D. Rasmussen, Nature **353**, 733 (1991).
[10]T. P. Martin, S. Bjørnholm, J. Borgreen, C. Bréchignac, Ph. Cahuzac, K. Hansen, and J. Pedersen, Chem. Phys. Lett. **186**, 53 (1991).
[11]C. Bréchignac, Ph. Cahuzac, F. Carlier, M. de Frutos, and J. Ph. Roux, Phys. Rev. B **47**, 2271 (1993).
[12]O. Genzken, M. Brack, E. Chabanat, and J. Meyer, Ber. Bunsenges. Phys. Chem. **96**, 1217 (1992).
[13]O. Genzken, Mod. Phys. Lett. B **7**, 197 (1993).
[14]T. Lange, H. Göhlich, T. Bergmann, and T. P. Martin, Z. Phys. D **19**, 113 (1991).
[15]T. P. Martin. T. Bergmann, H. Göhlich, and T. Lange, Chem. Phys. Lett. **172**, 209 (1990).
[16]J. Lermé, C. Bordas, M. Pellarin, B. Baguenard, J. L. Vialle, and M. Broyer, Phys. Rev. B **48**, 12 110 (1993).
[17]I. Katakuse, I. Ichihara, Y. Fujita, T. Matsuo, T. Sakurai, and H. Matsuda, Int. J. Mass Spectrom. Ion. Proc. **67**, 229 (1985).
[18]I. Katakuse, T. Ichihara, Y. Fujita, T. Matsuo, and H. Matsuda, Int. J. Mass. Spectrom. Ion. Proc. **69**, 109 (1986).
[19]M. Ruppel and K. Rademann, Chem. Phys. Lett. **197**, 280 (1992).
[20]H. Ito, T. Sakurai, T. Matsuo, T. Ichihara, and I. Katakuse, Phys. Rev. B **48**, 4741 (1993).
[21]K. E. Schriver, J. L. Persson, E. C. Honea, and R. L. Whetten, Phys. Rev. Lett. **64**, 2539 (1990); J. L. Persson, R. L. Whetten, H. P. Cheng, and R. S. Berry, Chem. Phys. Lett. **186**, 215 (1991).
[22]M. Pellarin, B. Baguenard, M. Broyer, J. Lermé, J. L. Vialle, and A. Perez, J. Chem. Phys. **98**, 944 (1993).
[23]J. Lermé, M. Pellarin, J. L. Vialle, B. Baguenard, and M. Broyer, Phys. Rev. Lett. **68**, 2818 (1992).
[24]B. Baguenard, M. Pellarin, C. Bordas, J. Lermé, J. L. Vialle, and M. Broyer, Chem. Phys. Lett. **205**, 13 (1993).
[25]M. Pellarin, B. Baguenard, C. Bordas, M. Broyer, J. Lermé, and J. L. Vialle, Phys. Rev. B **48**, 17 645 (1993).
[26]B. Baguenard, M. Pellarin, J. Lermé, J. L. Vialle, and M. Broyer, J. Chem. Phys. **100**, 754 (1994).
[27]Z. B. Güvenç and J. Jellineck, Z. Phys. D **26**, 304 (1993).
[28]H. S. Lim, C. K. Ong, and F. Ercolessi, Z. Phys. D **26**, 45 (1993).
[29]H. P. Cheng and R. S. Berry, Phys. Rev. A **45**, 7969 (1992).
[30]J. L. Martins, J. Buttet, and R. Car, Phys. Rev. B **31**, 1804 (1985).
[31]V. Bonacic-Koutecky, P. Fantucci, and J. Koutecky, Chem. Rev. **91**, 1035 (1991).
[32]U. Röthlisberger and W. Andreoni, J. Chem. Phys. **94**, 8129 (1991).
[33]M. P. Iñiguez, J. M. Lopez, J. A. Alonso, and J. M. Soler, Z. Phys. D **11**, 163 (1989).
[34]M. P. Iñiguez, J. A. Alonso, A. Rubio, M. J. Lopez, and L. C. Balbâs, Phys. Rev. B **41**, 5595 (1990).
[35]A. Mañanes, J. A. Alonso, U. Lammers, and G. Borstel, Phys. Rev. B **44**, 7273 (1991).
[36]D. M. Lindsay, Y. Wang, and T. F. George, J. Chem. Phys. **86**, 3500 (1987).
[37]J. Mansikka-aho, M. Manninen, and E. Hammaren, Z. Phys. D **21**, 271 (1991).
[38]P. Blaise, F. Spiegelmann, D. Maynau, and J. P. Malrieu, Phys. Rev. B **41**, 5566 (1990); R. Poteau and F. Spiegelmann, J. Chem. Phys. **98**, 6540 (1993).
[39]M. E. Spina and M. Brack, Z. Phys. D **17**, 225 (1990).
[40]T. P. Martin, U. Näher, and H. Schaber, Chem. Phys. Lett. **199**, 470 (1992).
[41]M. Manninen, J. Mansikka-aho, and E. Hammaren, Z. Phys. D **26**, 28 (1993).
[42]N. Pavloff and S. C. Creagh, Phys. Rev. B **48**, 18 164 (1993).
[43]K. Clemenger, Phys. Rev. B **32**, 1359 (1985).
[44]W. Ekardt and Z. Penzar, Phys. Rev. B **38**, 4273 (1988).
[45]S. M. Reimann, M. Brack, and K. Hansen, Z. Phys. D **28**, 235 (1993).
[46]O. Genzken and M. Brack, Phys. Rev. Lett. **67**, 3286 (1991).
[47]C. Guet and W. R. Johnson, Phys. Rev. B **45**, 11 283 (1992).
[48]A. Rubio, L. C. Balbas, and J. A. Alonso, Z. Phys. D **19**, 93 (1991).
[49]G. Lauritsch, P. G. Reinhard, J. Meyer, and M. Brack, Phys. Lett. A **160**, 179 (1991).
[50]T. Hirschmann, M. Brack, and J. Meyer, Ann. Phyz. (Leipzig) (to be published).
[51]K. K. Mon and D. Stroud, Phys. Rev. Lett. **45**, 817 (1980).
[52]M. Iwamatsu, J. Non-Cryst. Solids **156-158**, 826 (1993).
[53]N. D. Lang and W. Kohn, Phys. Rev. B **1**, 4555 (1970).
[54]J. W. Allen and S. A. Rice, J. Chem. Phys. **67**, 5105 (1977).
[55]T. P. Martin, T. Bergmann, H. Göhlich, and T. Lange, J. Phys. Chem. **95**, 6421 (1991).
[56]M. P. D'Evelyn and S. A. Rice, Phys. Rev. Lett. **47**, 1844 (1981).
[57]F. F. Abraham and Y. Singh, J. Chem. Phys. **67**, 2384 (1977).
[58]N. W. Ashcroft, Phys. Lett. **23**, 48 (1966).

[59]N. W. Ashcroft and D. C. Langreth, Phys. Rev. **155**, 682 (1967).
[60]N. W. Ashcroft and D. C. Langreth, Phys. Rev. **159**, 500 (1967).
[61]S. A. Blundell and C. Guet, Z. Phys. D **28**, 81 (1993).
[62]J. Lermé, C. Bordas, M. Pellarin, B. Baguenard, J. L. Vialle, and M. Broyer, Phys. Rev. B **48**, 9028 (1993).
[63]A. Rubio, L. C. Balbas, and J. A. Alonso, Solid State Commun. **75**, 139 (1990).
[64]K. Clemenger, Phys. Rev. B **44**, 12 991 (1991).
[65]V. Heine, M. L. Cohen, and D. Weaire, in *Solid State Physics,* edited by H. Ehrenreich, F. Seitz, and D. Turnbull (Academic, New York, 1970), Vol. 24, p. 1.
[66]A. Zunger and M. L. Cohen, Phys. Rev. Lett. **41**, 53 (1978).
[67]D. R. Hamann, M. Schlüter, and C. Chiang, Phys. Rev. Lett. **43**, 1494 (1979).
[68]G. B. Bachelet, D. M. Ceperley, and M. G. B. Chiochetti, Phys. Rev. Lett. **62**, 2088 (1989).
[69]G. B. Bachelet, D. R. Hamann, and M. Schlüter, Phys. Rev. B **26**, 4199 (1982).
[70]J. Mansikka-aho, M. Manninen, and H. Nishioka, Phys. Rev. B **48**, 1837 (1993).
[71]D. Ugarte, Z. Phys. D **26**, 150 (1993).
[72]P. G. Reinhard, S. Weisgerber, O. Genzken, and M. Brack, in *Nuclear Physics Concepts in Atomic Cluster Physics,* edited by R. Schmidt, H. O. Lutz, and R. Dreizler (Springer-Verlag, Berlin, 1992).
[73]O. Genzken, M. Brack, H. Bresele, G. Villing, and P. G. Reinhard (unpublished).
[74]L. Serra, G. B. Bachelet, N. Van Giai, and E. Lipparini, Phys. Rev. B **48**, 14 708 (1993).
[75]*Handbook of Chemistry and Physics,* 71st ed. (CRC, Boca Raton, FL, 1990), p. 12.1.